Supporting Information

Turning an Intrinsically Inefficient Reaction Efficient: Homogeneously Catalyzed Continuous-Flow Amination of Alcohols with Ammonia

Authors: Bernd Rienhoff,[1] Dario Nickel,[1] Sidonie Römer,[1] Niclas von Vietinghoff,[1] Dominik Pietschmann,[1] and Thomas Seidensticker,[1,*]

[1]TU Dortmund University, Department for Biochemical and Chemical Engineering, Laboratory of Industrial Chemistry, Emil-Figge-Straße 66, 44227 Dortmund, Germany

*Dr. Thomas Seidensticker, email: thomas.seidensticker@tu-dortmund.de, phone: +49 231 755 2310

Table of Contents

1. Utilized Chemicals and Reagents

Table S 1: Chemicals used in this work.

Chemical	Purity	Supplier / Manufacturer
Benzyl alcohol (1a)	99%	Carl Roth GmbH + Co. KG
2-fluorobenzyl alcohol (1b)	99%	BLD Pharmatech GmbH
4-fluorobenzyl alcohol (1c)	99%	BLD Pharmatech GmbH
2,4-difluorobenzyl alcohol (1d)	99%	BLD Pharmatech GmbH
Cyclopropylalcohol (1e)	95%	BLD Pharmatech GmbH
Tetrahydropyran-4-methanol (1f)	99%	BLD Pharmatech GmbH
Octanol (1g)	99%	ABCR
1,6-Hexanediol (1h)	97%	Fisher Scientific
Tyrosol (1i)	99%	BLD Pharmatech GmbH
$HRuCl(CO)(PPh_3)_3$	-	Fisher Scientific
Xantphos	98%	ABCR
***Tert*-Amyl alcohol**	98%	Fisher Scientific
Isooctane	99.5%	Carl Roth GmbH + Co. KG
Toluene	99%	Fisher Scientific
Ammonia	99.99%	Messer Industriegase GmbH
Argon	99.996%	Messer Industriegase GmbH
CO_2 (Carbon dioxide)	99.995%	Messer Industriegase GmbH

2. Materials and General Procedures

2.1. Flow-Setup

The flow reactor was built using four CETONI Nemesys Mid-Pressure Syringe pumps (5 mL, max. pressure 100 bar), a SHIMADZU GC-2010 Oven (30-450 °C) and a PRESSURE-TECH backpressure regulator (BP301-02-S-100-K-P-02N-BR, 0-100 bar). The capillary used had an inner diameter of 1 mm (1/16” outer diameter) and was made from stainless steel (1.4404). The reactor section located in the GC oven was 9 m long with a total volume of 7 mL. The temperature of the quenching water bath was regulated by a cryostat to 25 °C and a stainless-steel autoclave (300 mL) was utilized at the end of the setup as pressurized vessel for product collection.

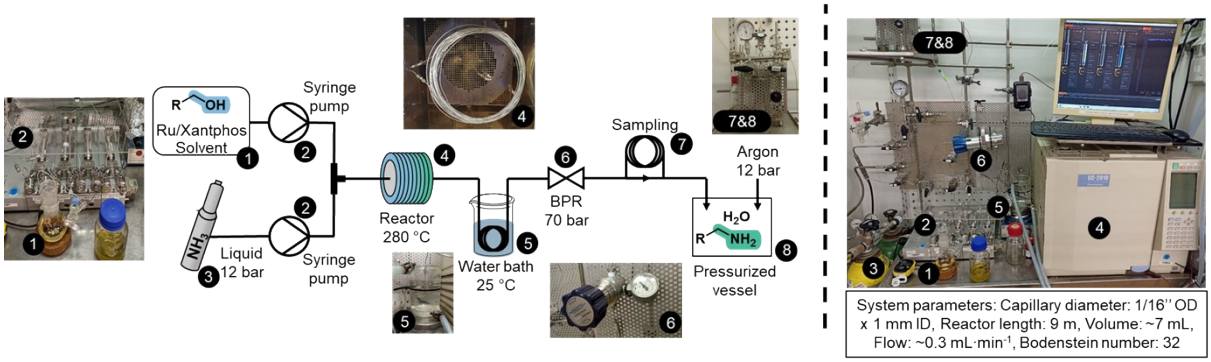

Figure S 1: Schematic illustration and recorded pictures of the utilized flow setup. 1) Substrate/Catalyst solution. 2) Syringe pumps. 3) Ammonia bottle. 4) Capillary reactor section in GC oven. 5) Water bath. 6) Back pressure regulator. 7) Sampling valve. 8) Pressurized vessel for product collection.

2.2. Experimental procedure

Solvents and liquid substrates were degassed in an ultrasonic bath under argon prior to use. The precursor $HRuCl(CO)(PPh_3)_3$ (3.2 mmol·L^{-1}) and Xantphos (6.4 mmol·L^{-1}) were placed in a Schlenk flask and inertized by three vacuum/argon cycles. Subsequently, *tert*-amyl alcohol and the substrate alcohol were added, and the mixture was refluxed under argon for one hour, during which the grey suspension transformed into a clear yellow solution. After cooling the solution to room temperature, it was used for the flow reaction.

The flow reactor was prepared by flushing the capillary with tert-amyl alcohol. Subsequently, the system was pressurized to 70 bar and the reactor temperature was set to the desired value. The catalyst solution and liquid ammonia were then introduced into the system using two of the four syringe pumps for each feed stream. Ammonia was withdrawn from a dip-tube cylinder at 12 bar, with argon serving as the pressurizing gas. The residence time and substrate-to-ammonia ratio were adjusted by varying the individual flow rates.

A T-fitting was utilized to merge the two streams before they entered the reactor section located in the heated GC oven. Afterwards, the reaction mixture was quenched in a temperature-controlled water bath (25 °C) and the pressure was reduced from 70 bar to 12 bar

with a back pressure regulator. At this stage, samples for GC analysis could be taken before the remaining reaction mixture was collected in a pressurized vessel.

2.3. Product isolation

Product isolation was performed with product mixtures collected under steady-state conditions between three and five residence times. The reaction solvent was removed and replaced by a solvent (mixture) as indicated in Table S 2. Crystallization of ammonium carbamate species and isolation of free amines was performed as described in literature.[1]

Table S 2: Utilized crystallization solvent and isolated yields for the studied amines.

Primary amine	Crystallization solvent	Isolated yield [%]
1b	Isooctane:Toluene (1:1)	57
2b	Isooctane:Toluene (1:2)	39
3b	Isooctane:Toluene (1:2)	43
4b	Isooctane:Toluene (1:2)	34
5b	-	-
6b	Isooctane	89
7b	Isooctane	74
8b	*tert*-amyl alcohol	15
9b	Isooctane:Toluene (1:1)	79

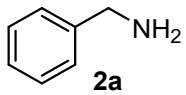

2a

The NMR spectroscopic data correspond to reported literature.[2]

^{1}H-NMR (400 MHz, Methanol-d_4): δ = 7.36 – 7.27 (m, 4H), 7.27 – 7.18 (m, 1H), 3.77 (s, 2H) ppm. ^{13}C-NMR (101 MHz, Methanol-d_4): δ = 143.65, 129.53, 128.42, 127.90, 46.72 ppm. GC-MS (EI, 70 eV): m/z (%) = 107.10 (100.00), 106.10 (61.13), 108.10 (61.02), 77.10 (38.36), 51.00 (33.70), 79.10 (32.56), 80.10 (28.20), 78.00 (27.61), 50.10 (22.54), 91.10 (18.00), 109.10 (14.07), 74.00 (13.47), 63.00 (11.08), 28.10 (10.98), 52.10 (10.56), 81.10 (10.48), 39.00 (10.27), 31.10 (10.23), 30.10 (9.58), 89.10 (8.71), 76.10 (8.64), 65.10 (8.38), 29.00 (7.73), 75.10 (7.32), 62.10 (6.19), 53.10 (5.71), 27.10 (5.44), 105.20 (5.36), 38.10 (5.05), 104.10 (3.96).

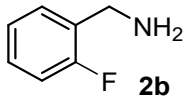

2b

The NMR spectroscopic data correspond to reported literature.[3]

^{1}H-NMR (400 MHz, Methanol-d_4): δ = 7.39 (td, *J* = 7.6, 1.8 Hz, 1H), 7.27 (tdd, *J* = 7.4, 5.3, 1.9 Hz, 1H), 7.14 (td, *J* = 7.5, 1.2 Hz, 1H), 7.06 (ddd, *J* = 10.5, 8.2, 1.2 Hz, 1H), 3.83 (s, 2H) ppm. ^{13}C NMR (101 MHz, Methanol-d_4): δ = 163.49, 161.06, 130.64 (d, J = 4.7 Hz), 129.89 (d, J = 8.3 Hz), 125.43 (d, J = 3.6 Hz), 116.10 (d, J = 21.9 Hz), 40.33 (d, J = 4.2 Hz) ppm. ^{19}F NMR (377 MHz, Methanol-d_4): δ = -122.01 – -122.11 (m, 1F) ppm. GC-MS (EI, 70 eV): m/z (%) = 106.10 (100.00), 107.10 (74.15), 79.00 (32.95), 77.00 (22.72), 108.00 (15.27), 78.10 (13.48), 91.10 (11.35), 124.00 (10.33), 80.00 (10.15), 51.10 (9.70), 28.10 (9.67), 105.20 (7.49), 49.90 (7.09), 104.00 (6.88), 89.00 (5.97), 30.10 (5.57), 109.00 (4.99), 281.00 (4.68), 65.00 (4.57), 125.10 (4.56), 63.00 (3.98), 76.00 (3.53), 74.00 (3.45), 52.00 (3.06), 97.10 (2.92), 29.20 (2.70), 38.90 (2.68), 74.90 (2.64), 52.90 (2.33), 75.20 (2.21).

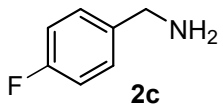

2c

The NMR spectroscopic data correspond to reported literature.[2]

^{1}H-NMR (400 MHz, Methanol-d_4): δ = 7.38 – 7.29 (m, 2H), 7.08 – 7.00 (m, 2H), 3.75 (s, 2H) ppm. ^{13}C-NMR (101 MHz, Methanol-d_4): δ = 164.50, 162.09, 139.74 (d, J = 3.2 Hz), 130.27 (d, J = 8.1 Hz), 116.06 (d, J = 21.4 Hz). ^{19}F-NMR (377 MHz, Methanol-d_4): δ = -118.47 (m, 1F) ppm. GC-MS (EI, 70 eV): m/z (%) = 124.10 (100.00), 105.10 (46.30), 97.00 (33.99), 125.10 (28.80), 75.00 (27.94), 109.00 (23.38), 95.10 (20.48), 77.10 (15.49), 96.10 (15.14), 28.10

(12.58), 30.10 (11.75), 83.00 (10.80), 74.00 (10.57), 104.10 (9.92), 50.10 (9.29), 107.10 (9.00), 122.00 (8.12), 51.00 (7.87), 78.00 (7.35), 106.10 (6.58), 69.00 (6.56), 57.00 (6.49), 70.00 (5.84), 76.00 (5.80), 94.10 (5.77), 63.00 (5.75), 81.10 (4.55), 68.00 (4.32), 62.00 (4.24), 89.00 (3.86).

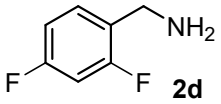

2d

The NMR spectroscopic data correspond to reported literature.[2]

^{1}H-NMR (400 MHz, Methanol-d_4): δ = 7.41 (p, *J* = 11.7, 10.2 Hz, 1H), 6.98 – 6.88 (m, 2H), 3.83 (s, 2H) ppm. ^{13}C NMR (101 MHz, Methanol-d_4): δ = 164.98, 163.57, 162.40, 161.12, 133.13, 131.89, 112.35, 112.31, 112.14, 112.10, 104.74, 104.48, 104.22, 39.61. ppm. ^{19}F-NMR (377 MHz, Methanol-d_4): δ = -113.96 (t, J = 8.1 Hz), -117.29 (d, J = 9.1 Hz) ppm. GC-MS (EI, 70 eV): m/z (%) = 143.00 (100.00), 144.10 (65.83), 123.10 (57.90), 142.10 (55.82), 127.00 (54.34), 124.10 (48.74), 63.00 (29.03), 75.00 (25.32), 113.00 (20.26), 114.00 (20.16), 125.00 (19.92), 101.00 (17.99), 95.00 (17.53), 107.00 (17.21), 115.00 (16.90), 31.10 (16.58), 96.00 (15.85), 116.00 (15.56), 74.10 (15.15), 122.10 (15.04), 29.10 (14.62), 28.10 (13.12), 145.10 (12.11), 81.10 (11.76), 62.10 (10.77), 93.00 (10.68), 94.00 (10.22), 30.10 (9.88), 51.00 (9.65), 50.00 (9.41).

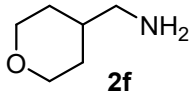

2f

The NMR spectroscopic data correspond to reported literature.[4]

^{1}H-NMR (400 MHz, Methanol-d_4): δ = 3.94 (ddt, *J* = 11.6, 4.7, 1.1 Hz, 2H), 3.41 (td, *J* = 11.9, 2.1 Hz, 2H), 2.51 (d, *J* = 6.6 Hz, 2H), 1.73 – 1.62 (m, 2H), 1.65 – 1.51 (m, 1H), 1.30 – 1.17 (m, 2H) ppm. ^{13}C-NMR (101 MHz, Methanol-d_4): δ = 68.86, 48.71, 39.04, 31.85 ppm. GC-MS (EI, 70 eV): m/z (%) = 31.10 (100.00), 30.10 (91.65), 55.10 (75.21), 29.10 (52.87), 39.10 (46.26), 71.10 (45.72), 72.10 (44.99), 67.10 (36.19), 56.10 (34.14), 28.10 (33.41), 57.10 (31.80), 41.10 (31.01), 53.10 (30.87), 32.10 (29.89), 54.10 (28.13), 27.10 (22.85), 44.10 (20.62), 43.10 (18.71), 68.10 (17.93), 42.10 (16.51), 69.10 (16.42), 58.10 (16.35), 70.10 (15.42), 73.10 (13.30), 87.10 (12.21), 51.10 (10.67), 88.10 (10.38), 40.10 (9.84), 59.10 (9.55), 83.10 (9.33).

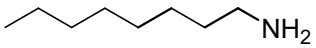

2g

The NMR spectroscopic data correspond to reported literature.[2]

^{1}H-NMR (400 MHz, Methanol-d_4) δ = 2.61 (t, J = 7.3 Hz, 3H), 1.53 – 1.40 (m, 2H), 1.40 – 1.24 (m, 10H), 0.90 (t, J = 6.7 Hz, 3H) ppm. ^{13}C-NMR (101 MHz, Methanol-d_4) δ = 42.64, 34.00, 33.04, 30.65, 30.44, 28.10, 23.74, 14.44 ppm. GC-MS (EI, 70 eV): m/z (%) = 30.10 (100.00), 41.10 (38.36), 39.10 (21.19), 29.20 (18.93), 43.10 (15.78), 42.10 (15.48), 86.10 (15.24), 27.10 (14.92), 55.10 (14.16), 28.10 (13.61), 44.10 (13.47), 56.10 (12.87), 69.10 (8.84), 100.10 (8.69), 45.10 (6.71), 53.10 (5.19), 54.20 (4.32), 130.20 (4.15), 70.10 (3.86), 72.10 (3.79), 129.20 (3.49), 67.10 (3.25), 83.10 (2.94), 128.20 (2.62), 57.20 (2.58), 26.10 (2.28), 51.10 (2.20), 59.10 (2.17), 68.10 (2.10), 31.00 (1.99).

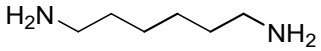

2h

The NMR spectroscopic data correspond to reported literature.[5]

^{1}H-NMR (400 MHz, Methanol-d_4) δ = 2.62 (t, J = 7.1 Hz, 4H), 1.52 – 1.43 (m, 4H), 1.38 – 1.33 (m, 4H) ppm. ^{13}C-NMR (101 MHz, Methanol-d_4): δ = 42.57, 33.95, 27.93 ppm. GC-MS (EI, 70 eV): m/z (%) = 30.10 (100.00), 56.10 (46.15), 87.10 (25.23), 70.10 (16.74), 42.10 (14.30), 86.10 (14.05), 28.10 (13.54), 44.00 (11.93), 41.10 (10.67), 100.20 (9.68), 43.10 (8.82), 69.10 (8.09), 59.10 (8.00), 45.00 (7.50), 55.10 (7.04), 99.20 (6.22), 39.10 (6.03), 72.10 (5.86), 57.10 (5.55), 31.00 (4.97), 98.00 (4.19), 82.10 (3.78), 73.10 (3.61), 29.00 (3.50), 67.00 (3.38), 27.00 (3.34), 54.10 (3.08), 81.10 (2.37), 53.10 (2.00), 88.10 (1.97).

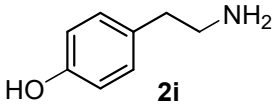

2i

The NMR spectroscopic data correspond to reported literature.[6]

^{1}H-NMR (400 MHz, Methanol-d_4): δ = 7.01 (d, J = 8.5 Hz, 2H), 6.71 (d, J = 8.5 Hz, 2H), 2.81 (t, J = 7.1 Hz, 2H), 2.64 (t, J = 7.2 Hz, 2H) ppm. ^{13}C-NMR (101 MHz, Methanol-d_4): δ = 157.12, 131.36, 130.70, 116.38, 44.33, 39.05 ppm. GC-MS (EI, 70 eV): m/z (%) = 108.10 (100.00), 107.00 (60.74), 109.00 (43.77), 77.10 (39.74), 30.10 (27.28), 78.00 (19.28), 31.10 (15.23), 79.10 (9.90), 137.10 (8.46), 91.10 (8.18), 138.00 (7.98), 110.10 (7.51), 51.00 (7.41), 53.10 (6.82), 80.10 (6.59), 63.10 (5.82), 52.00 (5.72), 39.10 (5.13), 65.00 (4.33), 50.10 (4.08), 81.10 (3.75), 28.20 (3.70), 92.10 (3.46), 90.00 3.23, 89.00 (3.15), 120.00 (2.91), 139.00 (2.87), 32.10 (2.75), 29.10 (2.71), 55.00 (2.57).

3. Analytics

3.1. NMR-Spectroscopy

^{1}H- and ^{13}C-NMR-spectra were recorded with a Bruker Avance III HD NanoBay - 400 MHz, Bruker Avance NEO – 500 MHz and Bruker Avance III HD – 600 MHz with the frequency and solvent noted. Chemical shifts δ are given in ppm relative to tetramethylsilane.

3.2. Gas Chromatography

GC analysis of reaction mixtures was performed on an Agilent Technologies INC. gas chromatograph G3950A equipped with a HP-5 column (30 m length, 0.32 mm diameter, 0.25 μm layer thickness) and a flame ionization detector (FID). The injection volume was 1 µL with a split ratio of 75:1. The temperature profile is given in Table S 2. Samples were prepared with 225 mg reaction solution, 25 mg n-dodecane (internal standard) and 750 mg isopropanol.

Table S 3: Temperature profile of the GC-FID method.

	Heating rate [°C·min^{-1}]	Value [°C]	Hold time [min]
Initial		40	5
Ramp 1	50	100	0
Ramp 2	25	200	0
Ramp 3	120	320	3

3.3. Inductively Coupled Plasma Optical Emission Spectrometry (ICP-OES)

ICP-OES analysis of phosphorus and ruthenium content was performed on a Plasma Quant PQ 9000 spectrometer.

4. Additional Results

4.1. Initial Investigation

The initial investigation was performed with a temperature screening using octanol (**1g**) as model substrate, due to its well-documented behavior in batch reactions. Highest reaction performance was observed at 280 °C and operation above this temperature led to reactor clogging caused by ruthenium black formation (Figure S 2). Further tests with benzyl alcohol (**1a**) at higher temperatures and reduced residence times confirmed that 280 °C represents the maximum stable operating temperature for this system (Figure S 4).

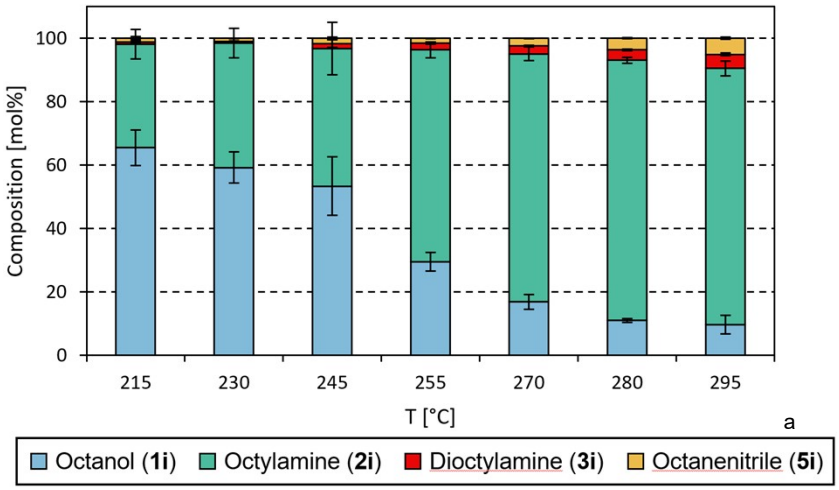

Figure S 2: Reaction results for the temperature screening of the alcohol amination of octanol (**1a**) with ammonia. Conditions: Octanol (225 mmol·L^{-1}) Ammonia:Octanol = 34:1 (mmol·mmol^{-1}), $HRuCl(CO)(PPh_3)_3$ (3.2 mmol·L^{-1}), Xantphos (6.4 mmol·L^{-1}), solvent = *tert*-amyl alcohol, p = 70 bar, τ = 33 min. Product distribution determined by GC-FID analysis with dodecane as internal standard. The values shown are mean values from three samples. The first sample was taken after 3.5·τ and the subsequent two samples were taken in 0.5·τ increments. a) Pressure constantly increasing and complete clogging of the reactor after four residence times.

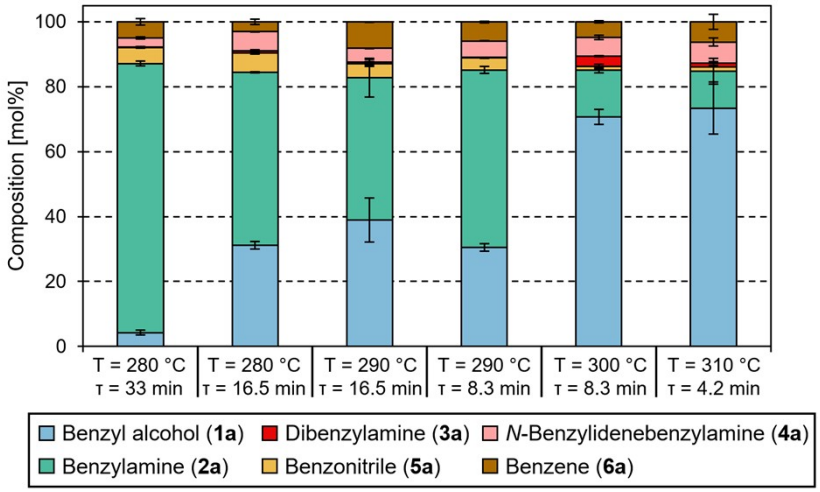

Figure S 3: Reaction results for the temperature screening of the alcohol amination of benzyl alcohol (**1b**) with ammonia. Conditions: Benzyl alcohol (261 mmol·L^{-1}), Ammonia:Alcohol = 34:1 (mmol·mmol^{-1}), $HRuCl(CO)(PPh_3)_3$ (3.2 mmol·L^{-1}), Xantphos (6.4 mmol·L^{-1}), solvent = *tert*-amyl alcohol, p = 70 bar. Product distribution determined by GC-FID analysis with dodecane as internal standard. The values shown are mean values from three samples. The first sample was taken after 3.5·τ and the following samples were taken in 0.5·τ increments. For all reactions above 280 °C pressure constantly increasing and complete clogging of the reactor after four residence times.

4.2. DoE Parameter Settings and Reaction Results

All experiments were performed as described in the experimental section and the optimization software Modde© was employed for the data evaluation. A central composite face-centered design with a quadratic model was selected as the experimental framework, resulting in a total of 17 experiments. The parameter settings and results are given in Table S 4. Notably: Experiments 18 to 22 were conducted in addition to the initial 17 optimization experiments with a higher benzyl alcohol (**1a**) concentration. The results of experiments 18, 21 and 22 were included in the prediction model.

Table S 4: Parameter settings and reaction results in the DoE.

Exp No	1a [mg·mL^{-1}]	Ratio NH_3:1a	τ [min]	Y [%]	S [%]	STY [mg mL^{-1} h^{-1}]	TON
1	14.3	13.5	13.3	82.55	85.30	52.91	40
2	43.0	13.5	13.3	59.85	80.63	115.14	92
3	14.3	54.1	13.3	63.63	72.38	40.79	36
4	43.0	54.1	13.3	58.79	72.77	113.10	100
5	14.3	13.5	53.2	85.45	86.11	13.46	41
6	43.0	13.5	53.2	79.48	81.80	37.58	121
7	14.3	54.1	53.2	75.70	76.61	11.92	41
8	43.0	54.1	53.2	68.14	71.24	32.22	119
9	14.3	33.8	33.3	84.01	84.93	21.25	41
10	43.0	33.8	33.3	72.19	76.59	55.55	117
11	28.7	13.5	33.3	80.62	87.12	41.34	77
12	28.7	54.1	33.3	72.25	73.09	37.05	82
13	28.7	33.8	13.3	76.49	81.17	98.06	78
14	28.7	33.8	53.2	81.60	82.97	26.15	82
15	28.7	33.8	33.3	80.84	83.29	41.45	80
16	28.7	33.8	33.3	81.01	84.04	41.54	80
17	28.7	33.8	33.3	80.48	83.92	41.27	79
18	57.4	13.5	13.3	50.28	74.95	128.94	111
19	57.4	54.1	13.3	71.65	73.37	183.74	162
20	57.4	13.5	53.2	87.56	88.13	55.18	165
21	57.4	54.1	53.2	76.74	77.11	48.36	165
22	57.4	33.8	33.3	71.00	81.95	72.83	144

Reaction conditions: $HRuCl(CO)(PPh_3)_3$ (3.2 mmol·L^{-1}), Xantphos (6.4 mmol·L^{-1}), solvent = *tert*-amyl alcohol, T = 280 °C, p = 70 bar, variable parameters as indicated. Results determined by GC-FID analysis with dodecane as internal standard. The values shown are mean values from three samples. The first sample was taken after3.5·τ and the subsequent two samples were taken in 0.5·τ increments. Note: All reactions with τ = 13.3 min showed pressure fluctuations and reactor clogging after four to five residence times.

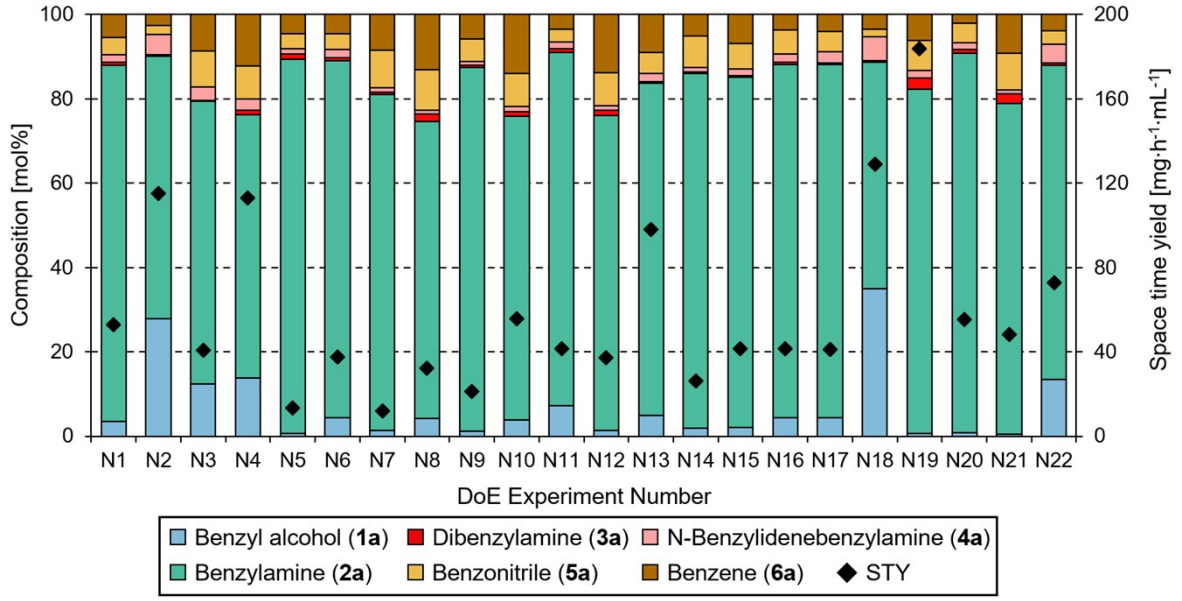

Figure S 4: Product compositions and STY of the DoE experiments. Reaction conditions see Table S 4.

Notably, pressure fluctuations were observed in all experiments with residence times of 13.3 min and clogging of the reactor occurred shortly after sampling. Including this system limitation, the residence time was manually adjusted to higher values during the subsequent optimum prediction in Modde©, to identify suitable conditions for continuous operation (Table S 5).

Table S 5: Predicted and observed results for optimized reaction conditions.

Entry	Value	Y [%]	S [%]	STY [mg·h^{-1}·mL^{-1}]	TON
Optimum prediction 1[a]	Predicted	77	84	58	-
	Observed	79	82	59	82
Optimum prediction 2[b]	Predicted	78	84	57	-
	Observed	76	81	56	62

Reaction conditions: $HRuCl(CO)(PPh_3)_3$ (3.2 mmol·L^{-1}), Xantphos (6.4 mmol·L^{-1}), solvent = *tert*-amyl alcohol, T = 280 °C, p = 70 bar. Product distribution determined by GC-FID analysis with dodecane as internal standard. a) Benzyl alcohol (273.63 mmol·L^{-1}), Ammonia:Alcohol = 18.3:1 (mmol·mmol^{-1}), τ = 23.3 min. b) Benzyl alcohol (209.08 mmol·L^{-1}), Ammonia: Alcohol = 16.9:1 (mmol·mmol^{-1}), τ = 18.3 min.

Experiments conducted at residence times of 23.3 min and 18.3 min demonstrated stable operation without pressure fluctuations. Furthermore, the experimental results showed good agreement with the model predicted values with a maximum deviation of 3%. Among the two selected conditions, optimum prediction 1 achieved superior results compared to optimum prediction 2 and was therefore used for further investigations (Table S 5).

4.3. Ruthenium and Phosphorus Contents

Table S 6: Measured ruthenium and phosphorus concentrations during the long-term experiment.

Time [h]	Initial	6	12	18	24	30
Ruthenium [ppm]	468	321	346	300	282	343
Phosphorus [ppm]	1074	1060	1116	1050	947	1077

Reaction conditions see long-term experiment. Ruthenium and phosphorus contents determined by ICP-OES analysis.

4.4. Results for the Catalyst Reuse

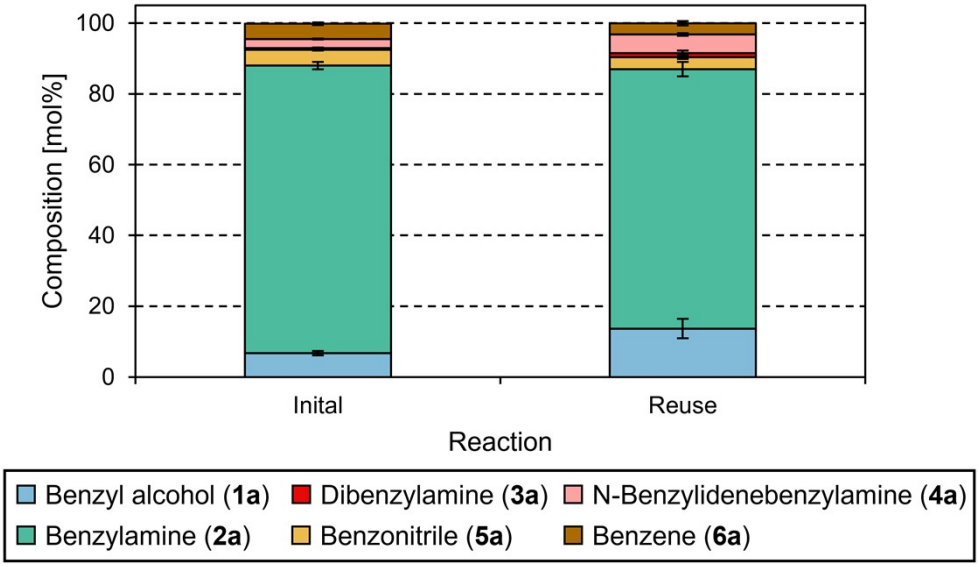

Figure S 5: Comparison of the reaction results of the initial and reused catalyst. Initial conditions: Similar to those of the long-term experiment, shown results are the average results from 16.5 h to 24 h. Reuse: A part of the product fraction of 16.5 h to 24 h was recharged with new benzyl alcohol (274 mmol·L^{-1}) and applied in another reaction. Product distribution determined by GC-FID analysis with dodecane as internal standard. The values shown are mean values from three samples. The first sample was taken after 3.5·τ and the following samples were taken in 0.5·τ increments.

4.5. Ammonia Solubility in *tert*-Amyl Alcohol

The solubility of ammonia in *tert*-amyl alcohol was investigated using a modified flow-view cell supplied by NieRuf GmbH (model GS03020003), which was operated as a static high-pressure visualization cell for monitoring the phase behavior during ammonia addition.

Prior to the experiment, the cell was pressurized with argon to 30 bar, after which *tert*-amyl alcohol (5 mL) was charged into the system. Ammonia was subsequently introduced stepwise under controlled conditions, and after each addition the system was allowed to equilibrate. The resulting phase behavior and the apparent solubility of ammonia in tert-amyl alcohol were visually assessed through the sight glass.

The experimental observations together with the corresponding phase behavior are summarized in Table S 7 and confirm complete miscibility under the applied conditions.

Table S 7: Results of the ammonia solubility in *tert*-amyl alcohol.

Entry	NH_3 [vol%]	NH_3 [wt%]	Monophasic?	Recorded picture
1	0	0	Yes	
2	10	7.7	Yes	
3	20	15.8	Yes	
4	30	24.4	Yes	
5	40	33.4	Yes	
6	50	43.0	Yes	

Conditions: *Tert*-amyl alcohol (5 mL), Ammonia (0 – 50 vol%, stepwise addition), p = 30 bar, T = 21.7 °C. After each addition the system was allowed to equilibrate before the resulting phase behavior was recorded.

4.6. Blind-Activity Test Example

The experiments were performed as described in Chapter 2.2, except that the catalyst precursor $HRuCl(CO)(PPh_3)_3$ was not added to the reaction solution. The cumulative amount of detected side products in all blank experiments remained consistently below 1%.

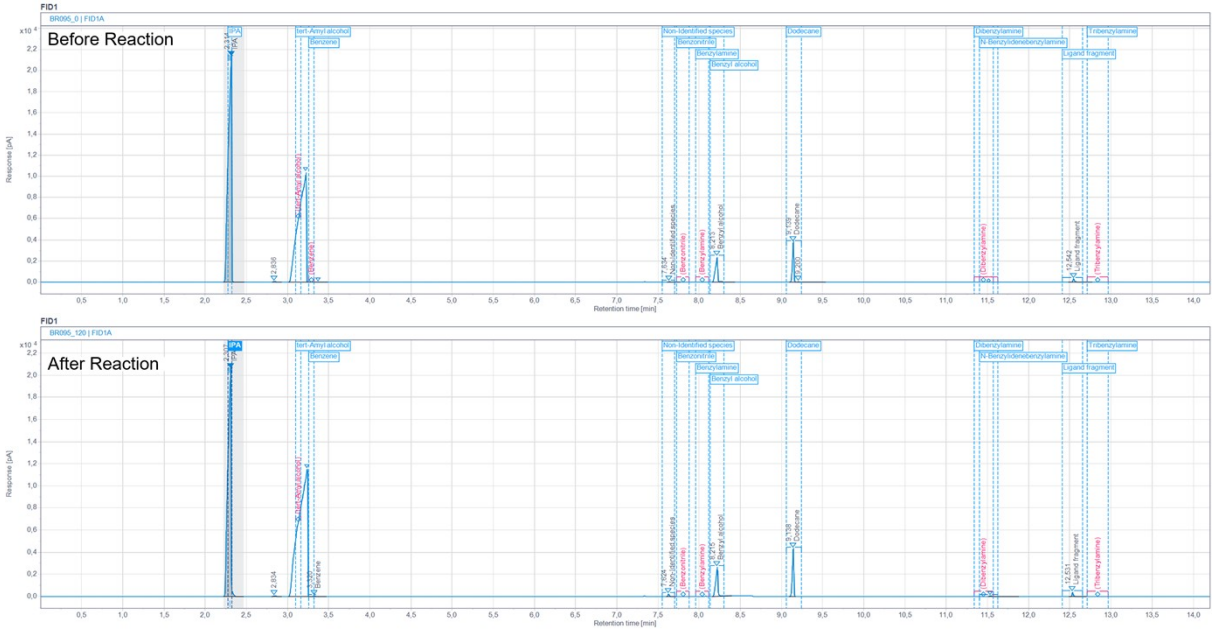

Figure S 6: Recorded pictures of GC-FID chromatograms of a catalytic blind test experiment before (top) and after reaction (bottom).

4.7. Residence Time Distribution

The aim was to analyze the residence time distribution of the reactor section r(t) under reaction conditions. As the peripheral equipment is required to maintain these conditions, the cumulative residence time curve of the reactor section could not be measured in isolation. Instead, r(t) was obtained as the residual signal by subtracting the cumulative residence time curve of the periphery g(t) (setup without the reactor section), from that of the full setup f(t). The procedure is described and illustrated stepwise in Figure S 7. In practice, r(t) was determined as the inverse transfer function obtained from the ratio of the Laplace transforms of the full setup signal f(t) and the periphery signal g(t).[7–9]

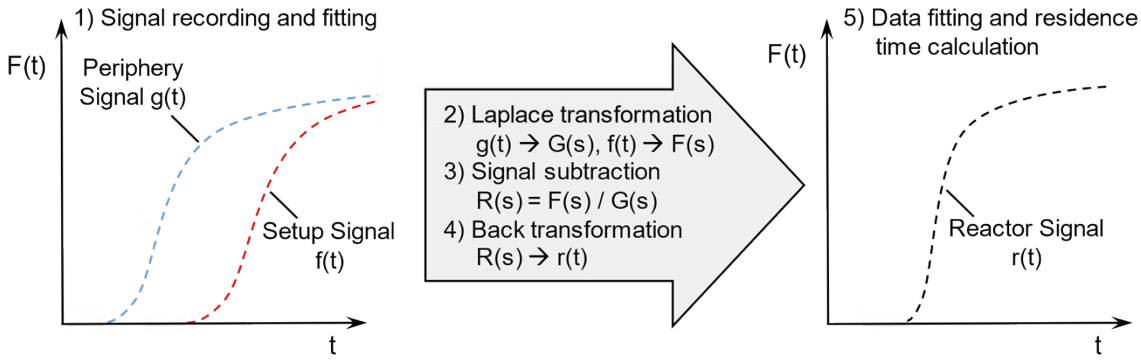

Figure S 7: Illustration of the procedure for the residence time analysis of the reactor section.

In Step 1, signal recording for both cumulative residence time curves f(t) and g(t) was performed using tetradecane as inert tracer (step signal). The measurement conditions were identical to those of the long-term experiment, and the tracer concentration was adjusted to match that of the alcohol substrate. After data acquisition, the measured data points for g(t) and f(t) were fitted using formula (2), where K is a scaling constant set to 1 (corresponding to the maximum of the cumulative residence time cumulative curve), b represents the time correction shift on the x-axis, and T_1 and T_2 are variable factors to fit the best approximation.

$$y(t) = K \cdot \left(1 - \frac{T_1}{T_1 - T_2} e^{\frac{-(t+b)}{T_1}} + \frac{T_2}{T_1 - T_2} e^{\frac{-(t+b)}{T_2}}\right) \tag{2}$$

Steps 2-4 were performed using a Python script provided in section 4.8. The fitted curves were transferred into the frequency domain with a Laplace transformation and then subtracted from one another. Afterwards the residual signal was back-transformed into the time domain to obtain the cumulative residence time curve of the reactor section (Figure S 8).

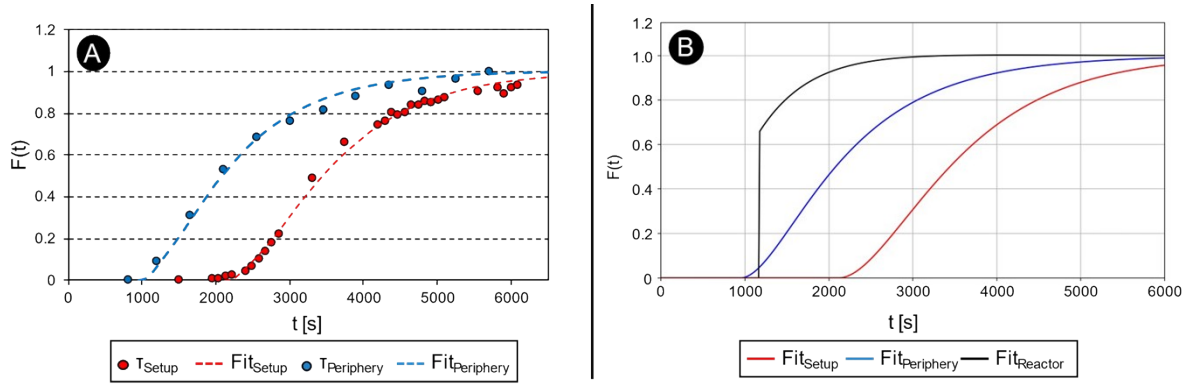

Figure S 8: Residence time measurement, fitting and python output. A) Measured residence time cumulative curves and their fits according to formula (2). Fit_{Setup}: K = 1, b = 2120, T_1 = 760, T_2 = 815. $Fit_{Periphery}$: K = 1, b = 950, T_1 = 990, T_2 = 410. B) Python output for the fitted periphery, setup and the calculated reactor residence time cumulative curves.

In Step 5 (Figure S 7), the resulting data points for the reactor section were plotted (Figure S 9) and fitted using *Origin*© to determine F(t) of the reactor (see formula (3)). The residence time (τ) was subsequently calculated using formula (4), yielding a value of 22.7 minutes, corresponding to a deviation of 2.6% from the theoretical residence time of 23.3 minutes.

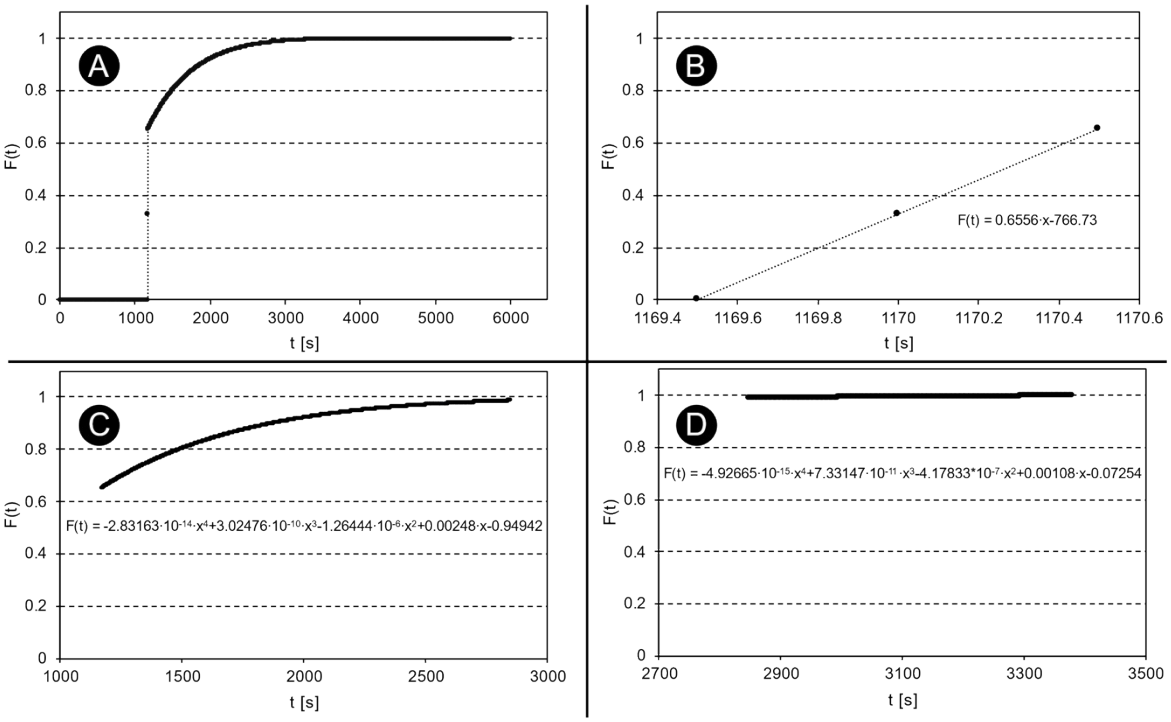

Figure S 9: Plotted reactor residence time cumulative curve A and fitted sections B to D.

$$F(t) = \begin{cases} 0 & \text{for } 0 \le t < 1169.5 \\ 0.6556 \cdot x - 766.73 & \text{for } 1169.5 \le t < 1170.5 \\ -2.83163 \cdot 10^{-14} \cdot x^4 + 3.02476 \cdot 10^{-10} \cdot x^3 - 1.26444 \cdot 10^{-6} \cdot x^2 + 0.00248 \cdot x - 0.94942 & \text{for } 1170.5 \le t < 2847 \\ -4.92665 \cdot 10^{-15} \cdot x^4 + 7.33147 \cdot 10^{-11} \cdot x^3 - 4.17833 * 10^{-7} \cdot x^2 + 0.00108 \cdot x - 0.07254 & \text{for } 2847 \le t < 3380.5 \end{cases} \quad (3)$$

$$\tau = \int_0^{\infty} (1 - F(t))dt = \sum_i \int_{a_i}^{b_i} \left(1 - F_i(t)\right)dt \quad (4)$$

In addition to the residence time, the Bodenstein number (Bo) was derived from F(t) according to formulas (5 to 8), resulting in a value of 32.

$$Bo = \frac{1 + \sqrt{1 + 8\sigma^2}}{\sigma^2} \quad (5)$$

$$\sigma^2 = \frac{\mu_2}{\tau^2} \quad (6)$$

$$\mu_2 = \int_0^{\infty} (t-\tau)^2 E(t)dt = \sum_i \int_{a_i}^{b_i} (t-\tau)^2 E_i(t)dt \quad (7)$$

$$E(t) = \frac{dF(t)}{dt} \quad (8)$$

4.8. Python Script (Residence Time Calculation)

```
import numpy as np
import sympy as sp
import matplotlib.pyplot as plt
import pandas as pd
import openpyxl
import os

# Define symbolic variables
t, s = sp.symbols('t s')

# Function parameters (Periphery)
a1 = 950  # Time shift
A_1 = 990 # Fit Parameter T1
B_1 = 410 # Fit Parameter T2

# Periphery transfer function G(s)
G_s = sp.exp(-a1 * s) / ((1 + s * A_1) * (1 + s * B_1))

# Function parameters (Setup)
a2 = 2120  # Time shift
A_2 = 760  # Fit Parameter T1
B_2 = 815  # Fit Parameter T2

# Setup transfer function F(s)
F_s = sp.exp(-a2 * s) / ((1 + s * A_2) * (1 + s * B_2))

# Calculation reactor transfer function in Laplace domain R(s)
R_s = F_s / G_s

# Back transformation in time domain g(t), f(t), r(t)
```

```
g_t = sp.inverse_laplace_transform(G_s / s, s, t)
f_t = sp.inverse_laplace_transform(F_s / s, s, t)
r_t = sp.inverse_laplace_transform(R_s / s, s, t)

# Numerical evaluation for plotting and exporting to excel
t_start = 0     # Start time
t_step = 1    # Time step size
t_end = 6000    # End time

t_eval = np.arange(t_start, t_end + t_step, t_step)   # Generate time points

g_numeric_values = [float(g_t.subs(t, ti)) for ti in t_eval]
f_numeric_values = [float(f_t.subs(t, ti)) for ti in t_eval]
r_numeric_values = [float(r_t.subs(t, ti)) for ti in t_eval]

#Define path to save data (replace desktop path with the path to the desired storage location)
os.chdir('C:/Users/smberien/Desktop')

# Exporting to Excel file using pandas DataFrame and ExcelWriter functionality.
print('Export started')
data_to_export = pd.DataFrame({'Time': t_eval,
                               'Periphery': g_numeric_values,
                               'Reactor': r_numeric_values,
                               'Setup': f_numeric_values})

#Replace name with your desired file name
data_to_export.to_excel("Export_file_residence_time.xlsx", index=False)

print("Data has been successfully exported.")

#Plotting results
print('Start plotting')
plt.figure(1)
plt.plot(t_eval, g_numeric_values, 'b', label='Periphery')
plt.plot(t_eval, r_numeric_values, 'k', label='Reactor')
plt.plot(t_eval, f_numeric_values, 'r', label='Setup')
plt.axis([0, t_end, 0, max(f_numeric_values)*1.2])
```

```
plt.legend(loc='lower right')
plt.xlabel('Time (t)')
plt.ylabel('Amplitude')
plt.title('System Response')
plt.grid()
plt.show()
```

5. NMR Spectra

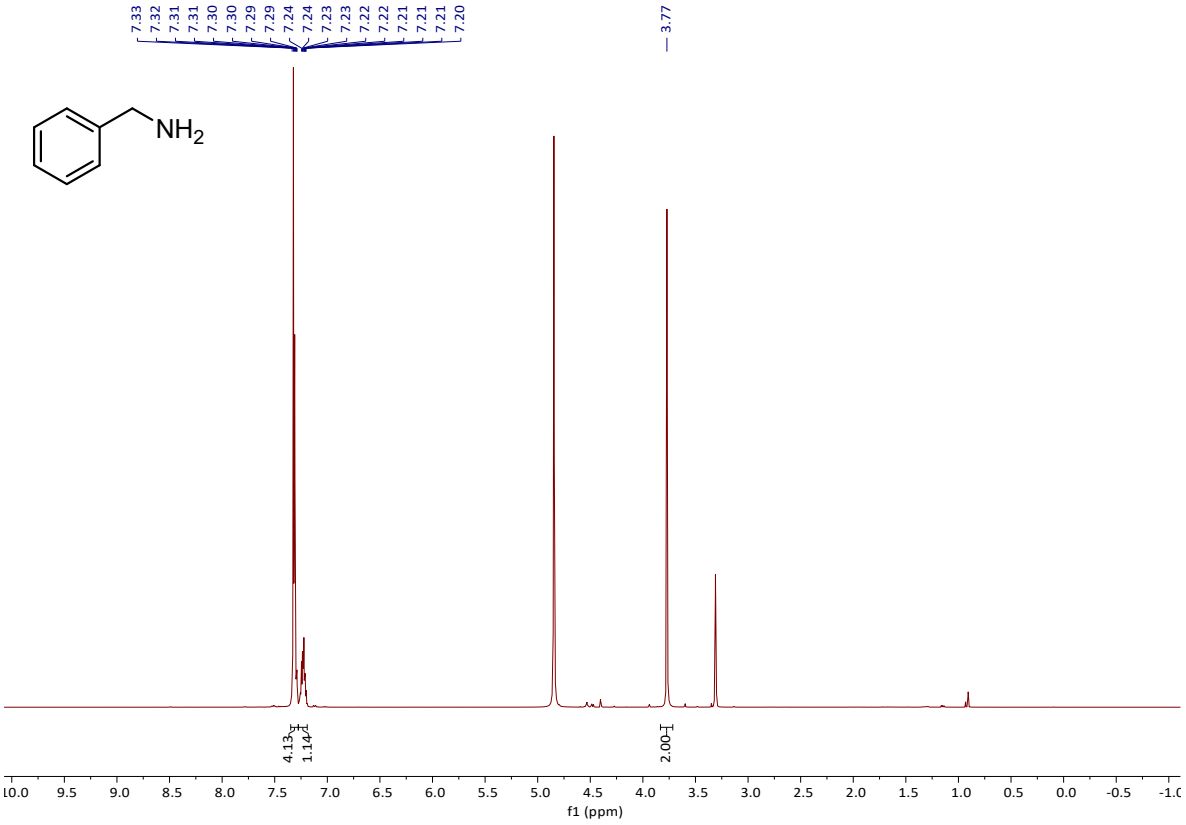

Figure S 10: ^{1}H-NMR (400 MHz, Methanol-d_4) of benzylamine (**2a**).

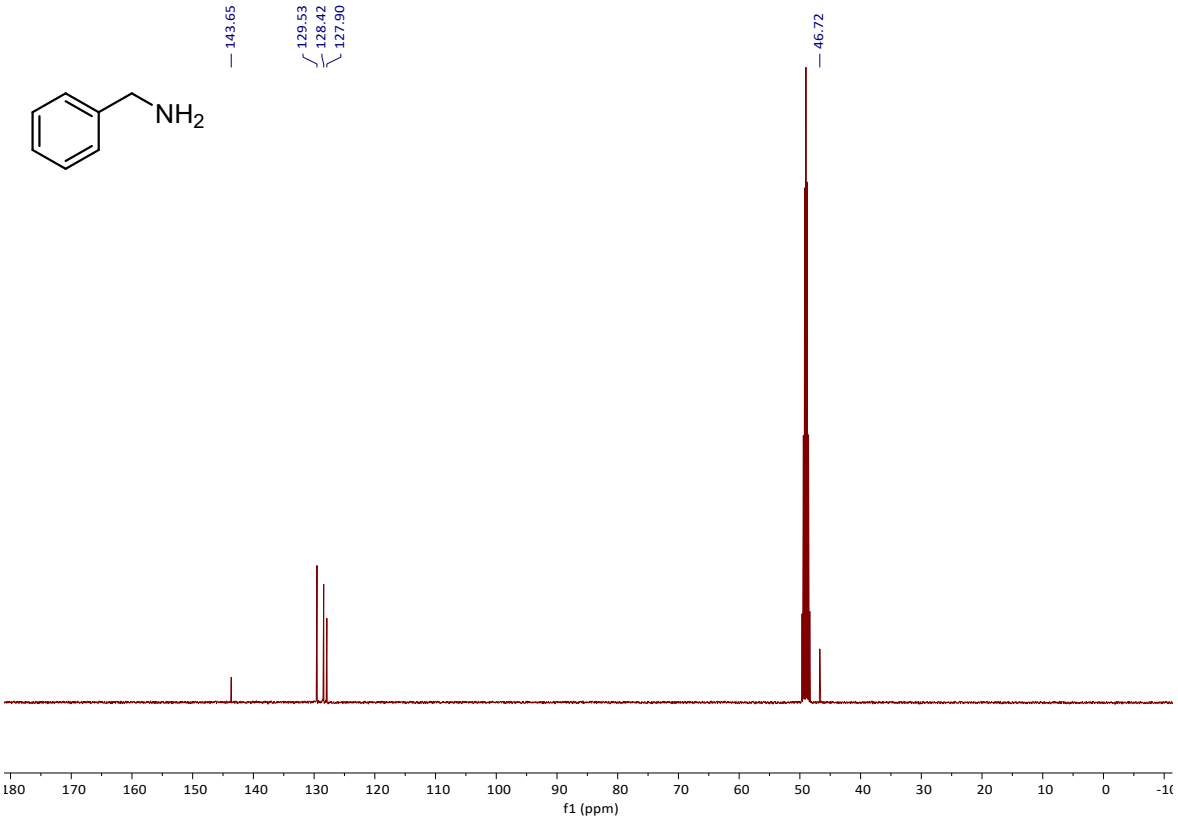

Figure S 11: ^{13}C-NMR (101 MHz, Methanol-d_4) of benzylamine (**2a**).

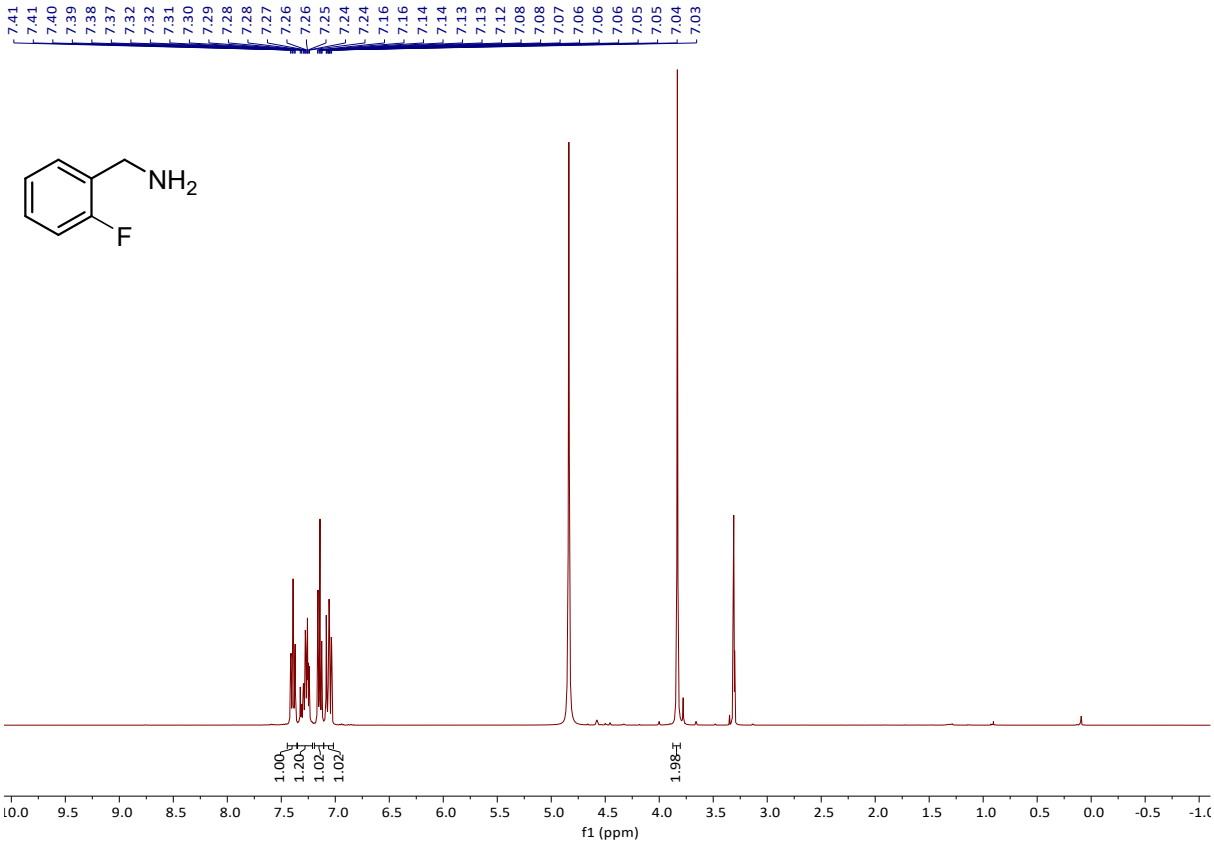

Figure S 12: ^{1}H-NMR (400 MHz, Methanol-d_4) of 2-fluorobenzylamine (**2b**).

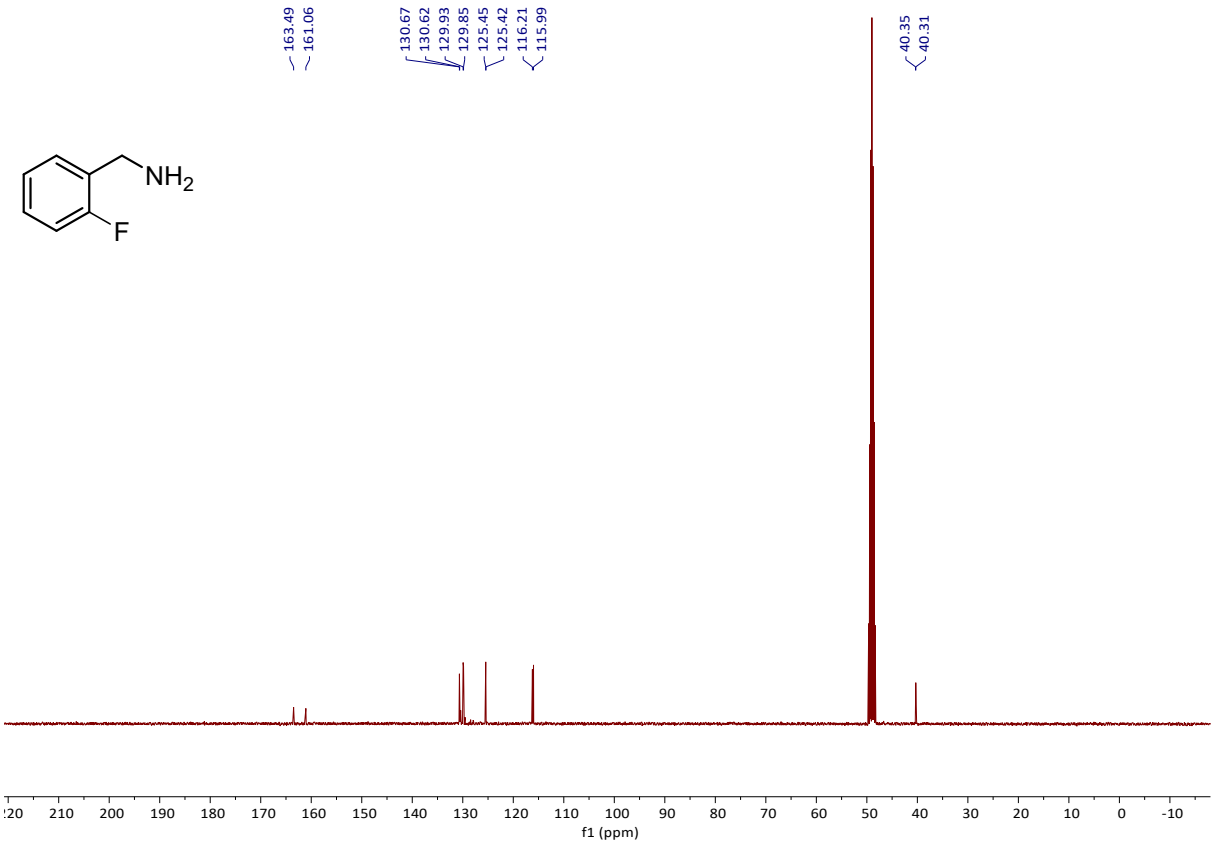

Figure S 13: ^{13}C-NMR (101 MHz, Methanol-d_4) of 2-fluorobenzylamine (**2b**).

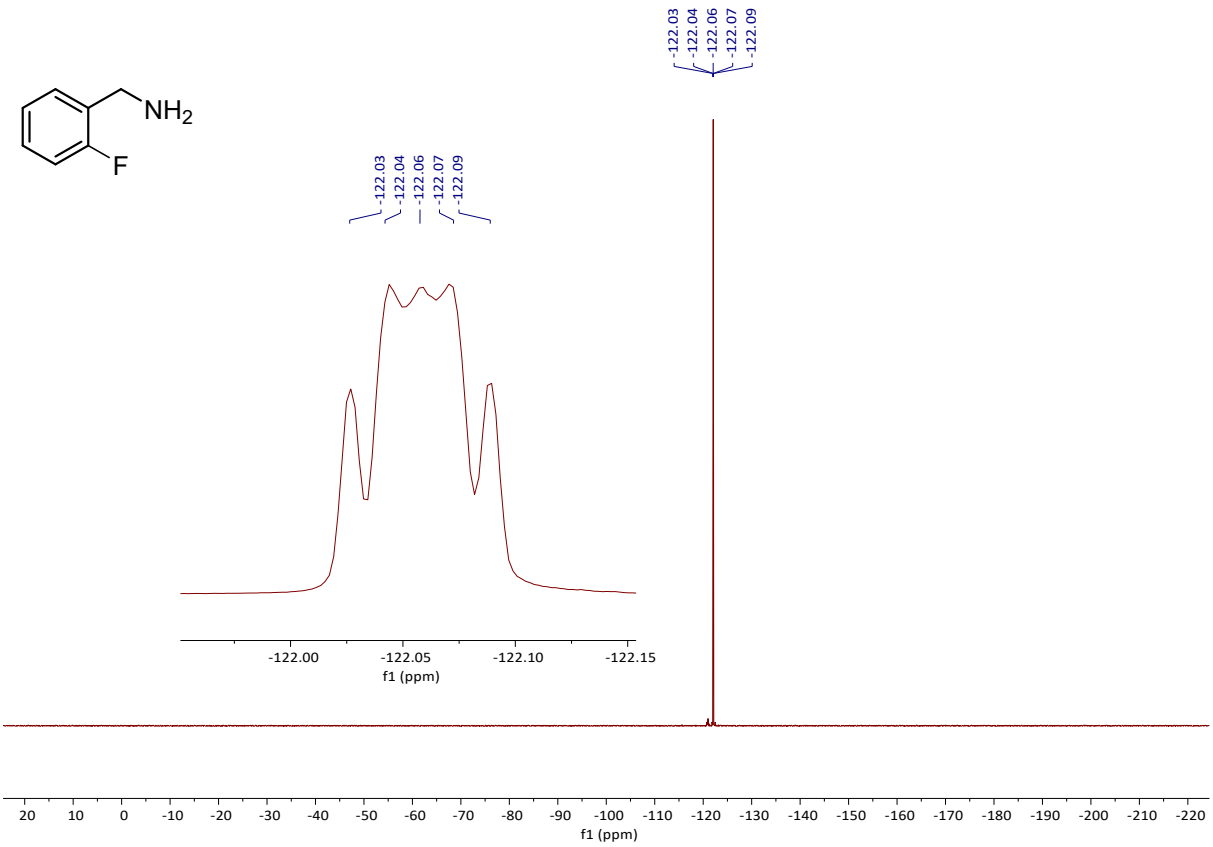

Figure S 14: ^{19}F-NMR (377 MHz, Methanol-d_4) of 2-fluorobenzylamine (**2b**).

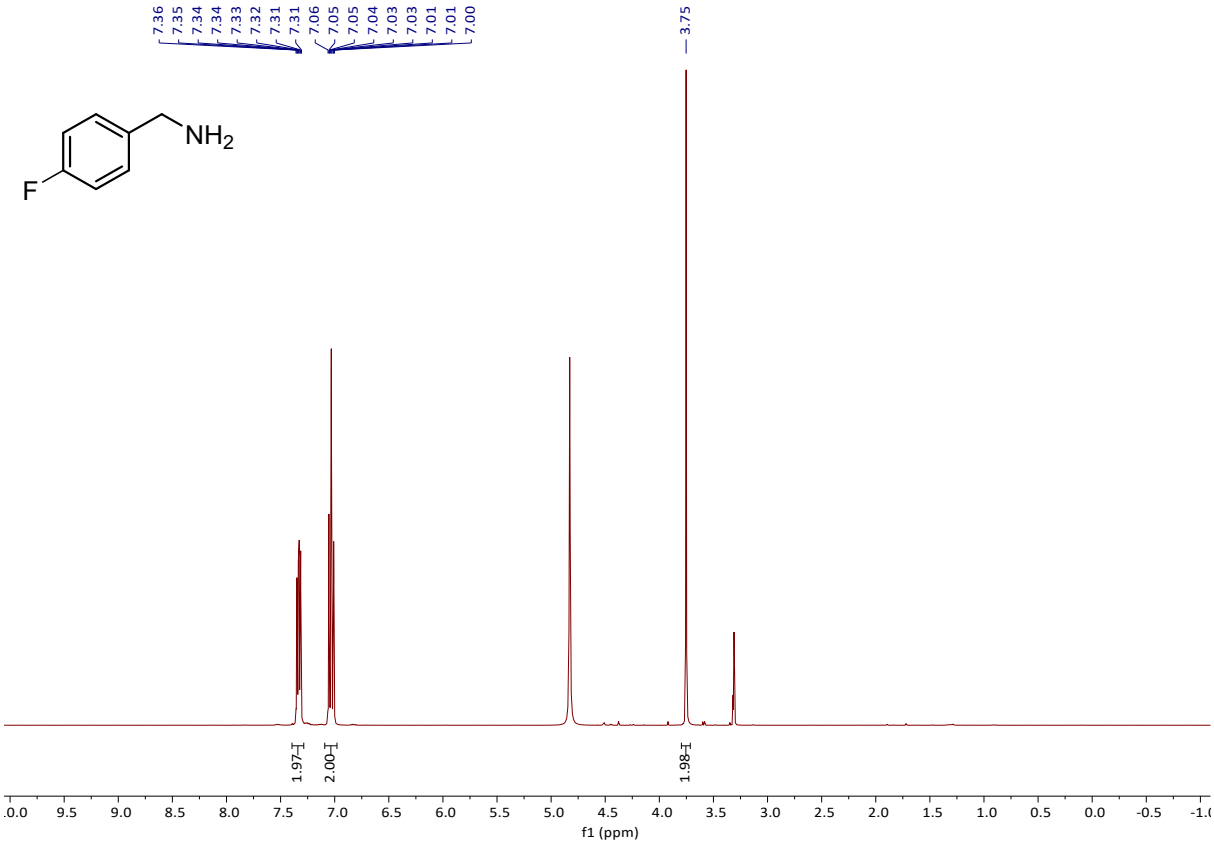

Figure S 15: ^{1}H-NMR (400 MHz, Methanol-d_4) of 4-fluorobenzylamine (**2c**).

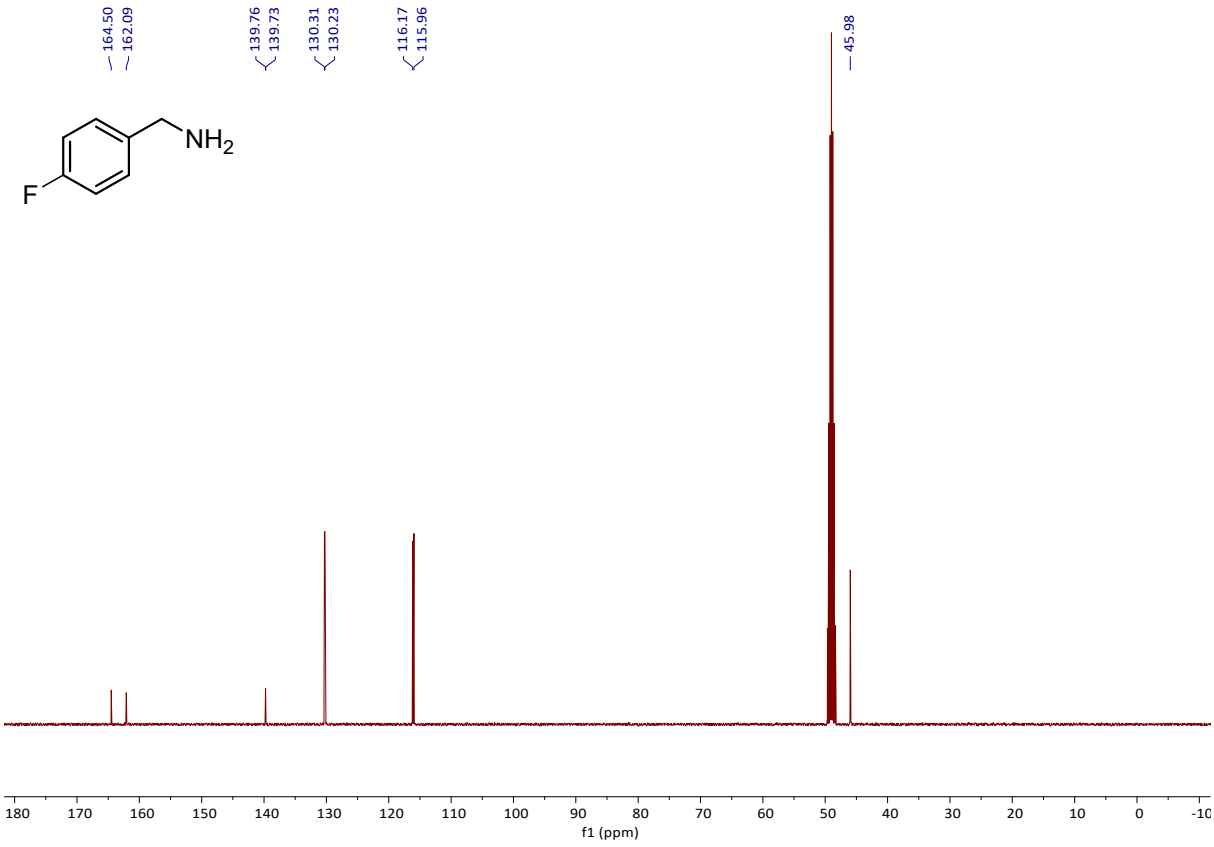

Figure S 16: ^{13}C-NMR (101 MHz, Methanol-d4) of 4-fluorobenzylamine (**2c**).

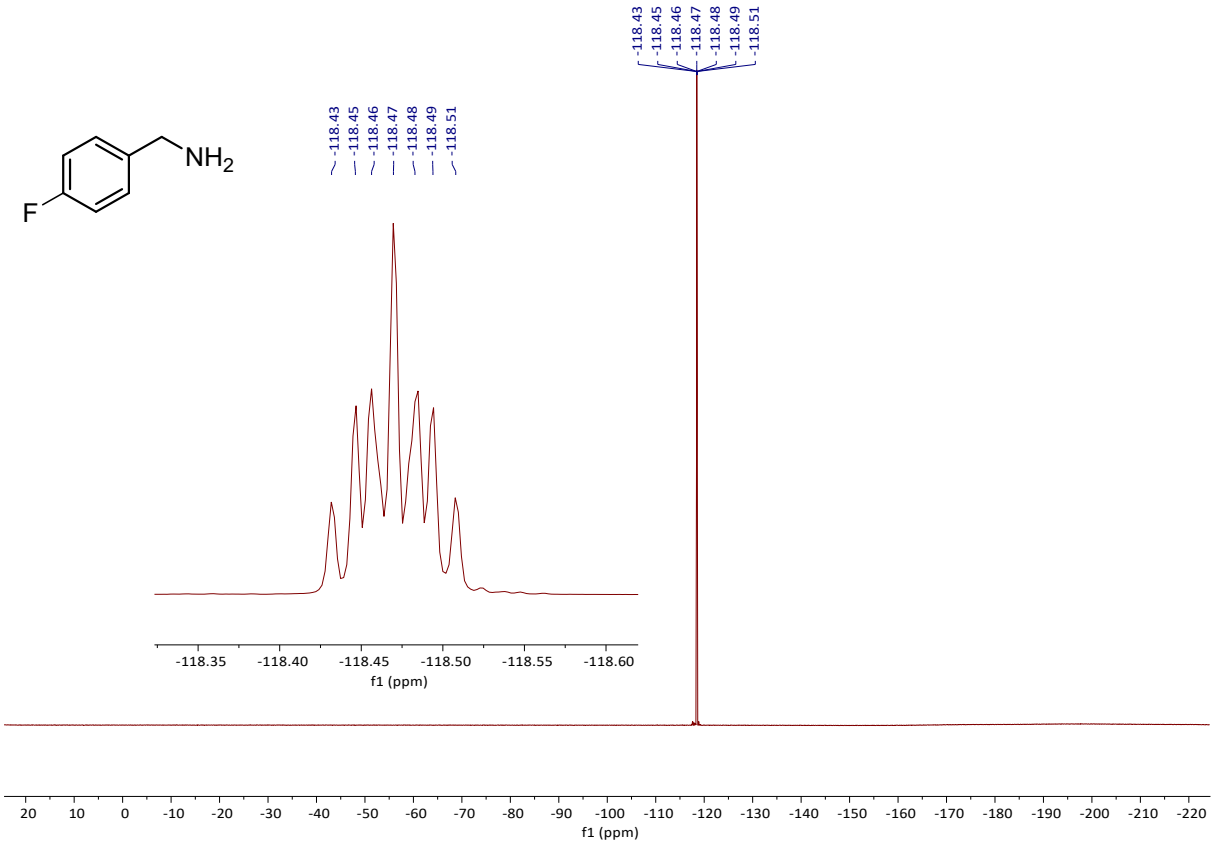

Figure S 17: ^{19}F-NMR (377 MHz, Methanol-d_4) of 4-fluorobenzylamine (**2c**).

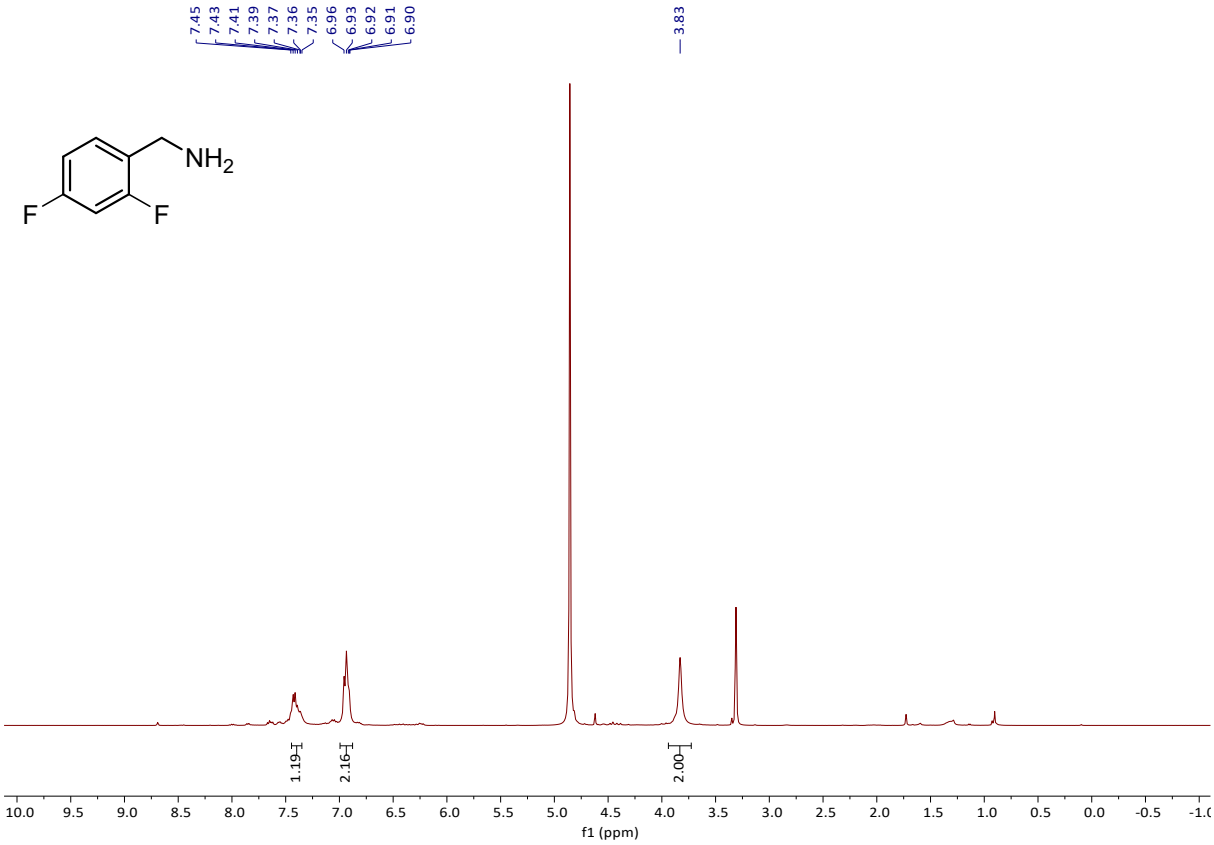

Figure S 18: ^{1}H-NMR (400 MHz, Methanol-d_4) of 2,4-difluorobenzylamine (**2d**).

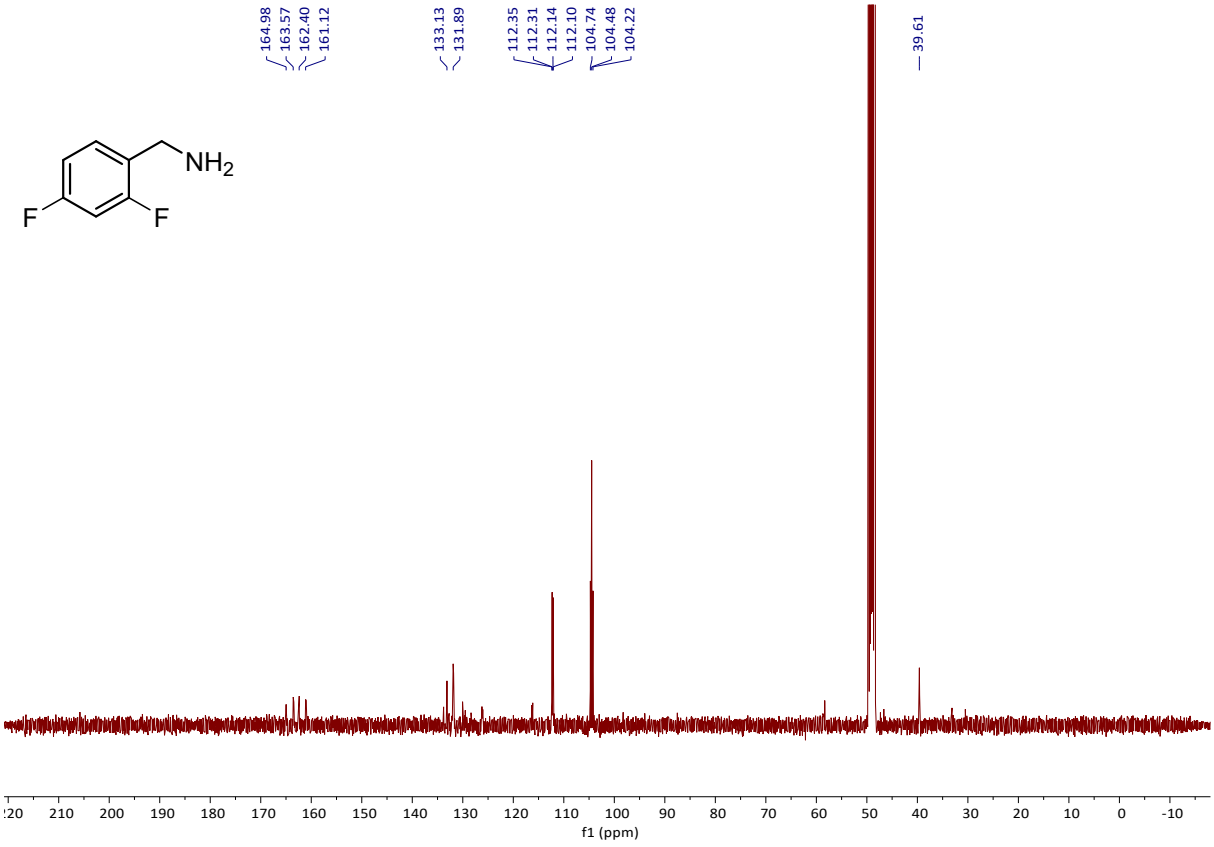

Figure S 19: ^{13}C-NMR (101 MHz, Methanol-d_4) of 2,4-difluorobenzylamine (**2d**).

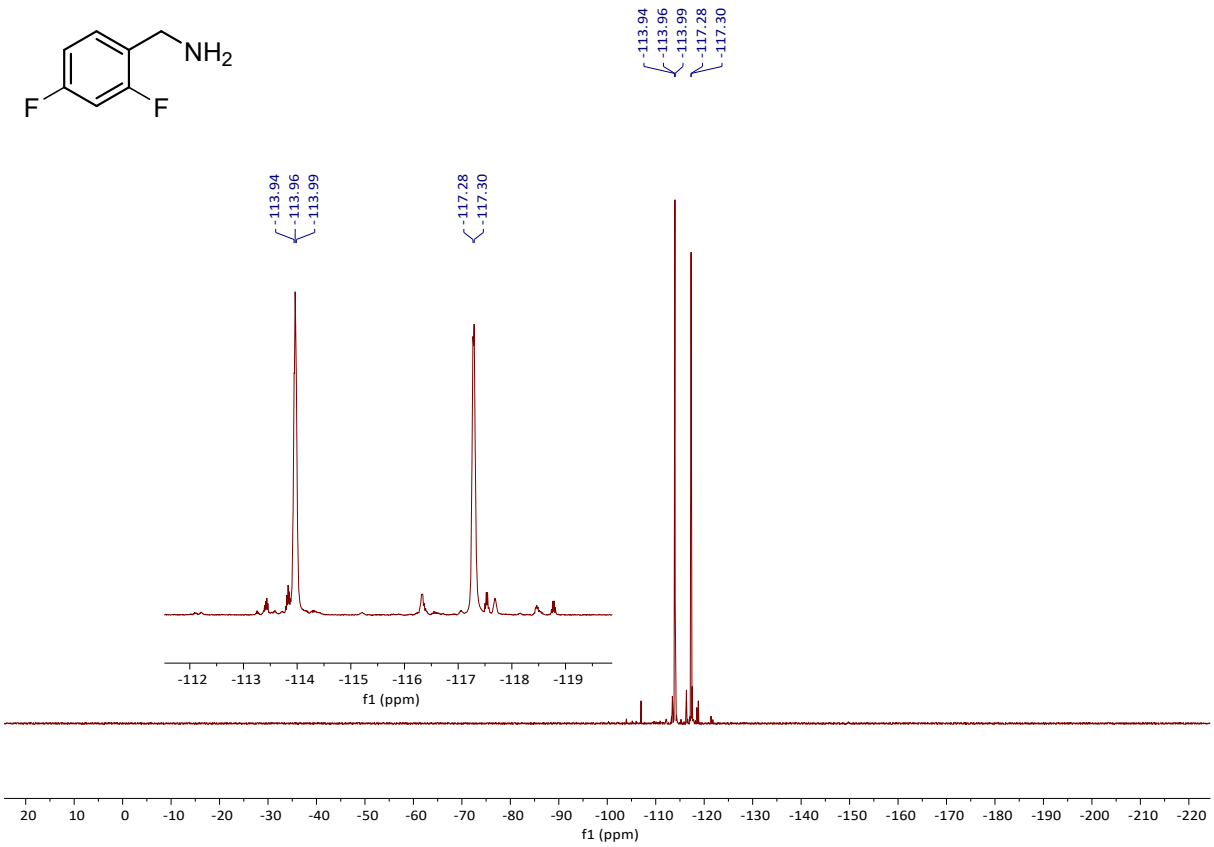

Figure S 20: ^{19}F-NMR (377 MHz, Methanol-d_4) of 2,4-difluorobenzylamine (**2d**).

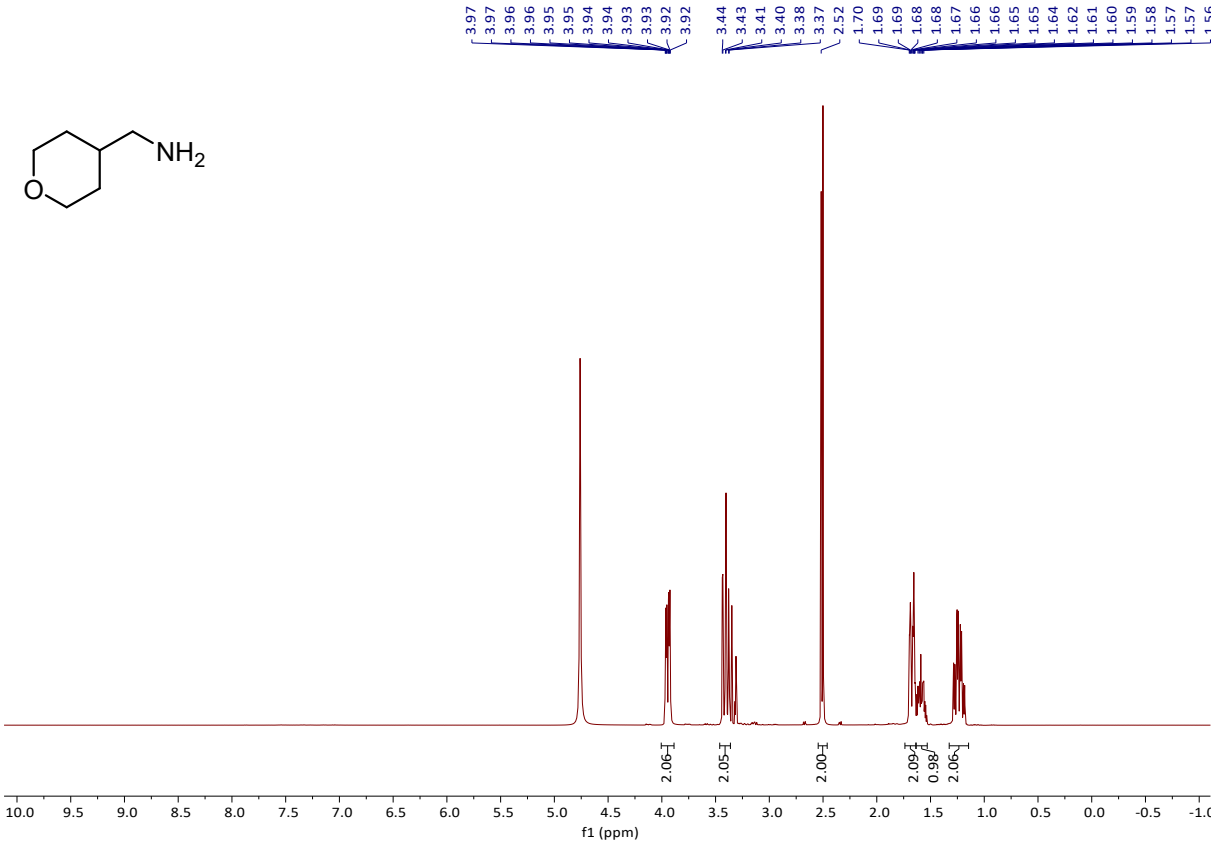

Figure S 21: ^{1}H-NMR (400 MHz, Methanol-d_4) of 4-tetrahydropyranmethylamine (**2f**).

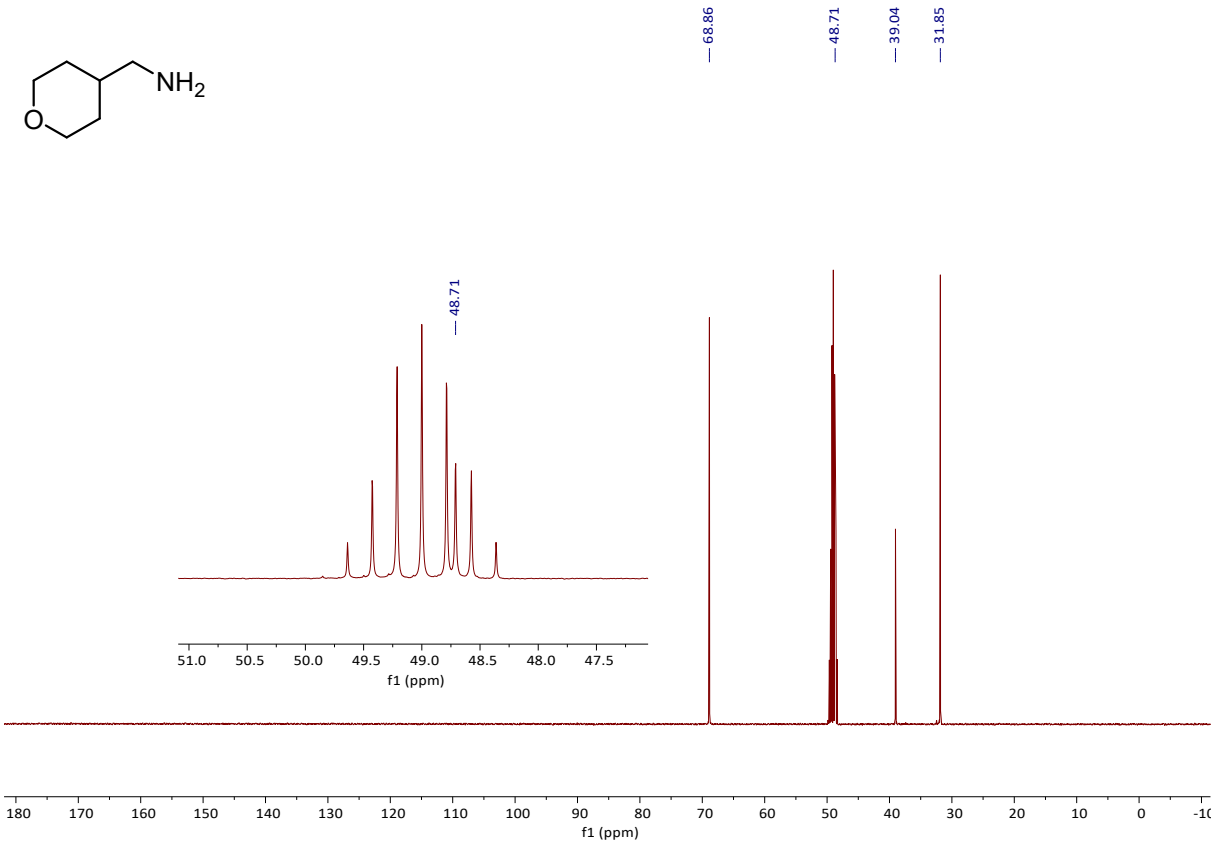

Figure S 22: ^{13}C-NMR (101 MHz, Methanol-d_4) of 4-tetrahydropyranmethylamine (**2f**).

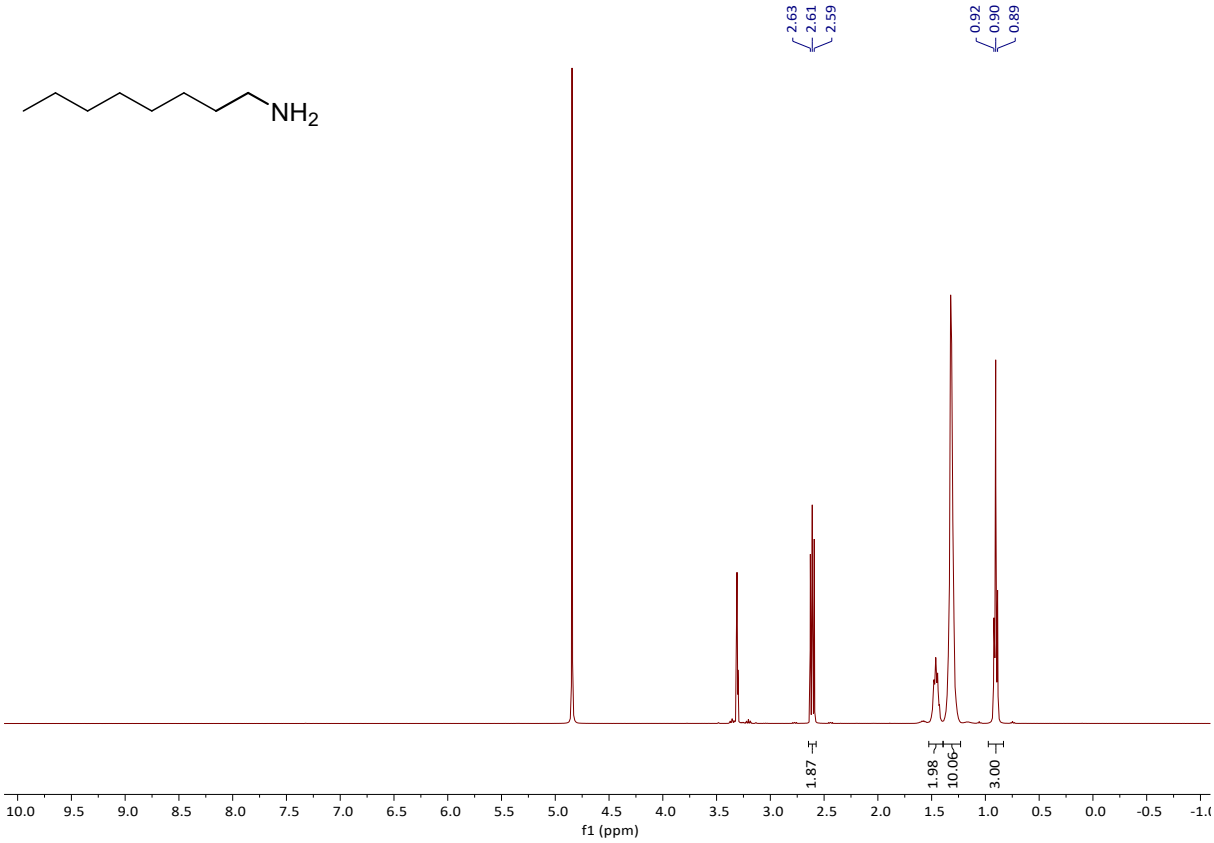

Figure S 23: ^{1}H-NMR (400 MHz, Methanol-d_4) of octylamine (**2g**).

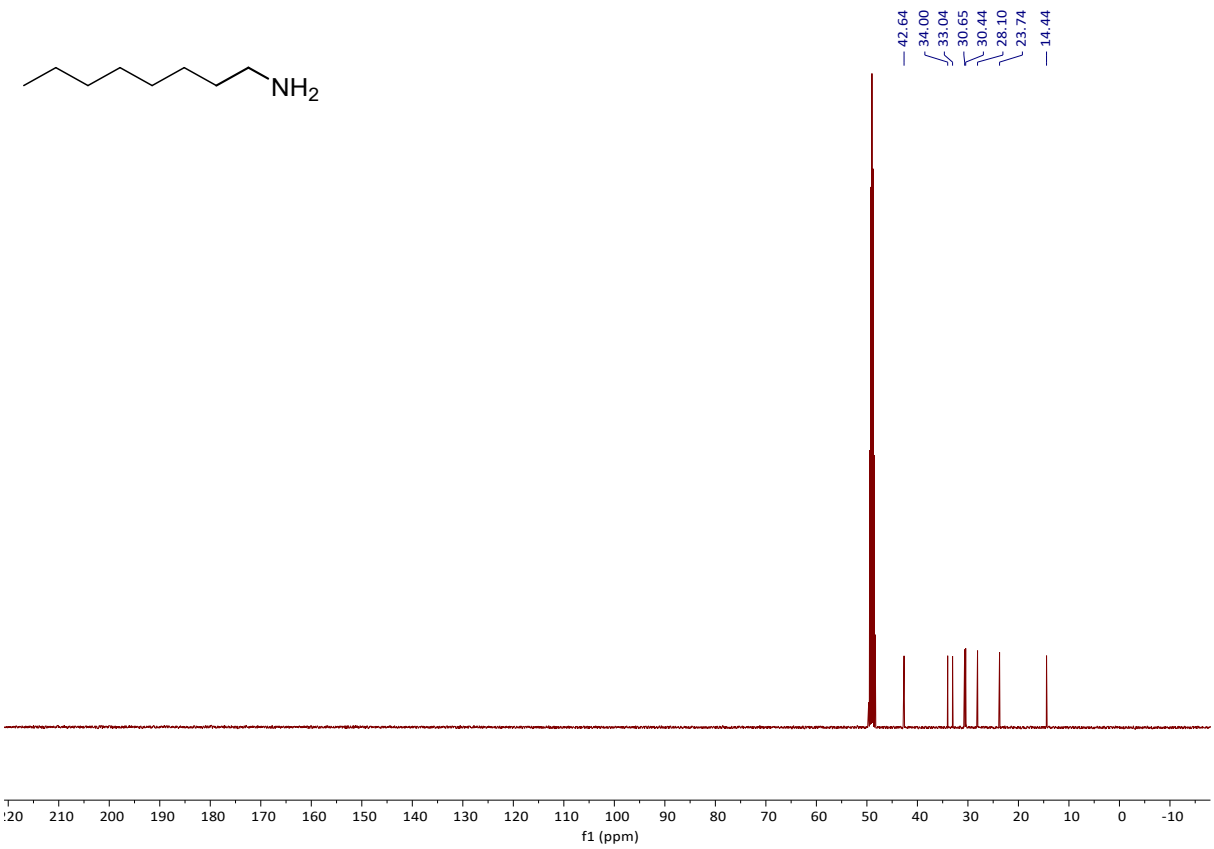

Figure S 24: ^{13}C-NMR (101 MHz, Methanol-d_4) of octylamine (**2g**).

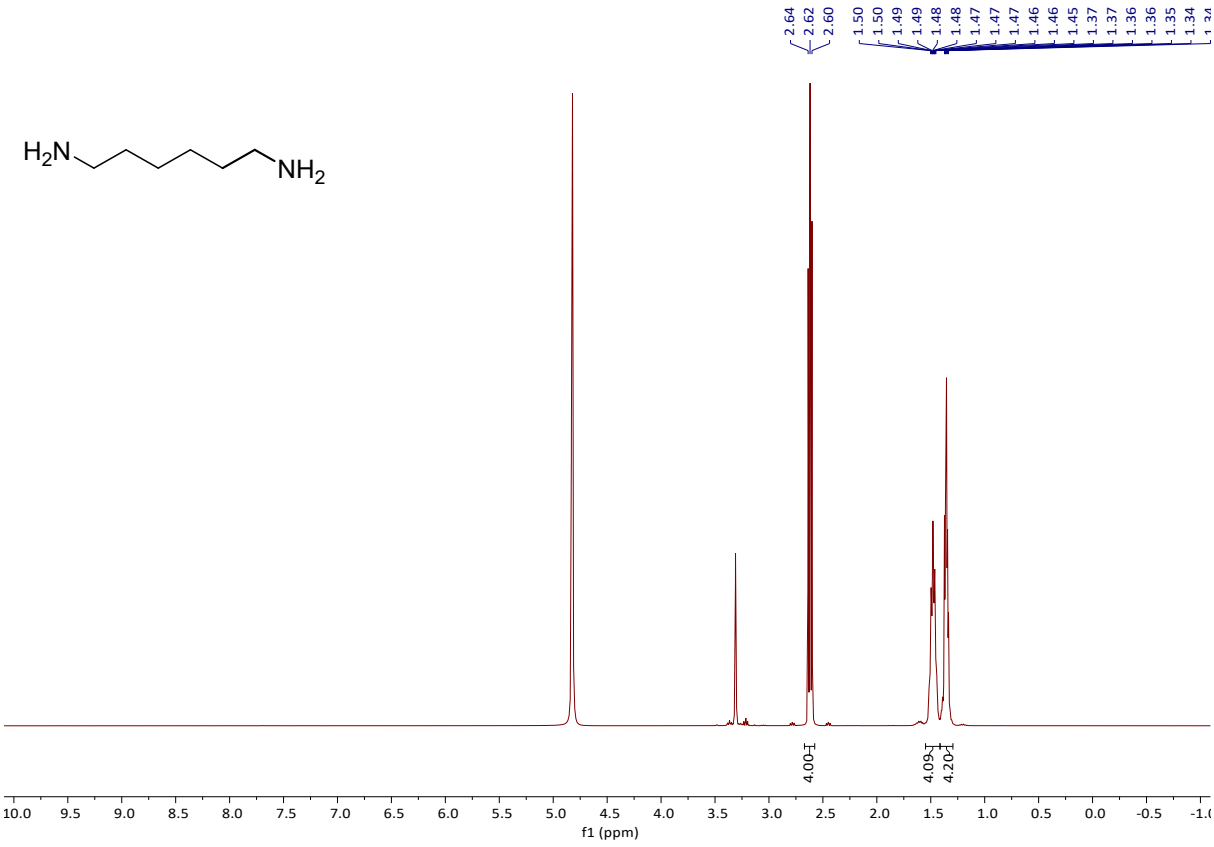

Figure S 25: ^{1}H-NMR (400 MHz, Methanol-d_4) of 1,6-hexamethylenediamine (**2h**).

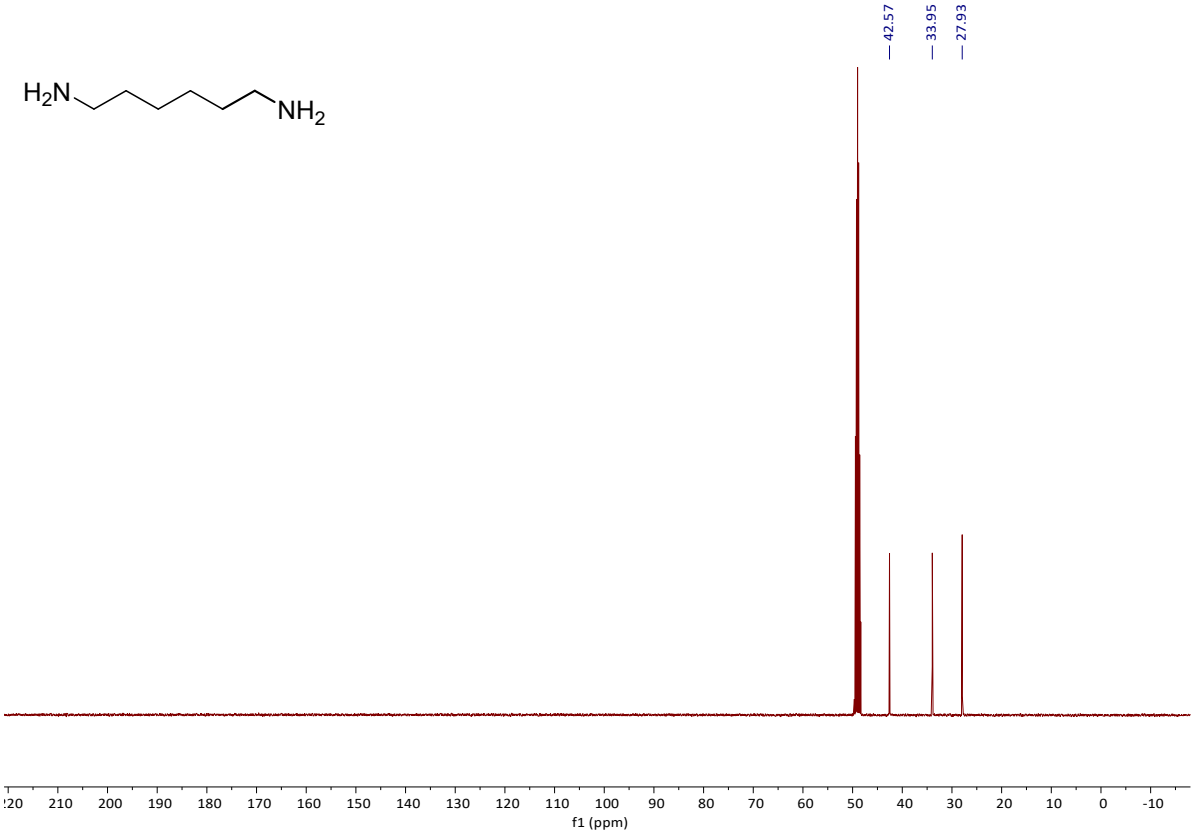

Figure S 26: ^{13}C-NMR (101 MHz, Methanol-d_4) of 1,6-hexamethylenediamine (**2h**).

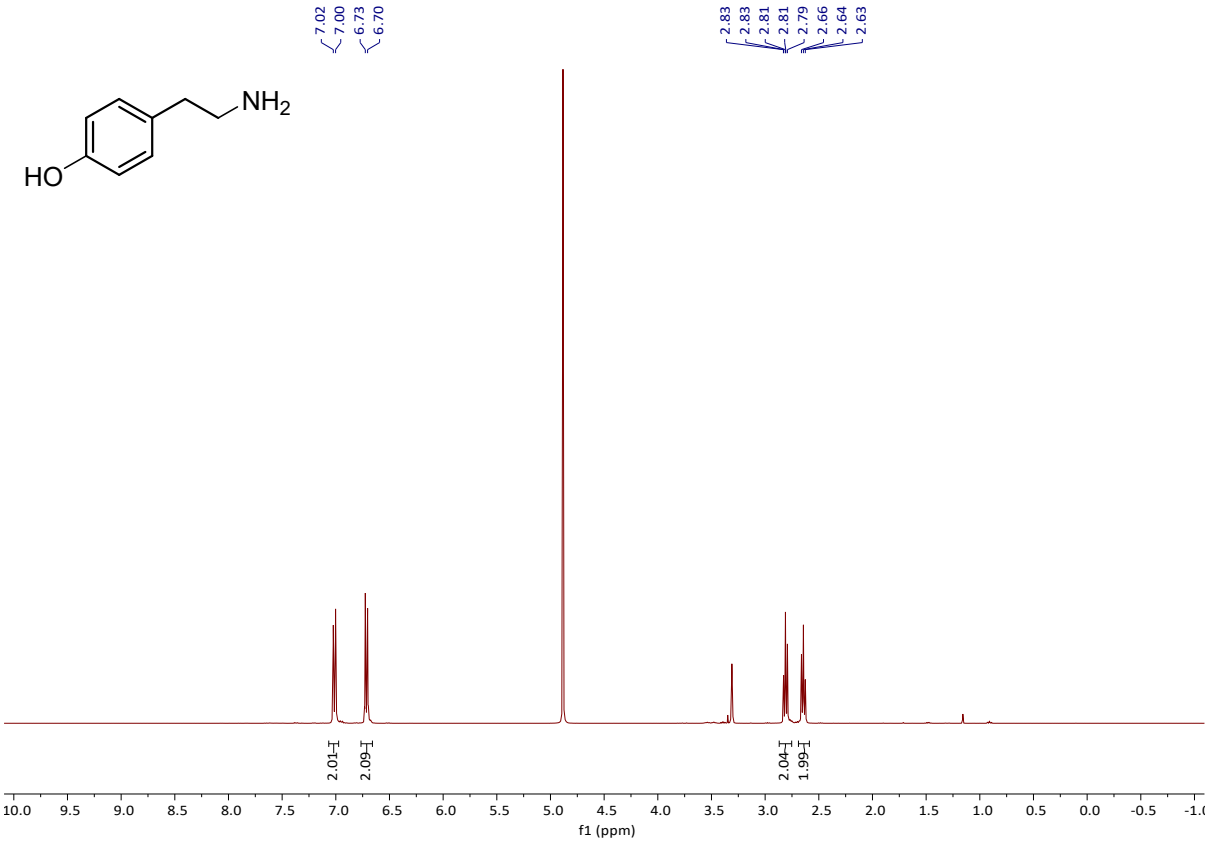

Figure S 27: ^{1}H-NMR (400 MHz, Methanol-d_4) of tyramine (**2i**).

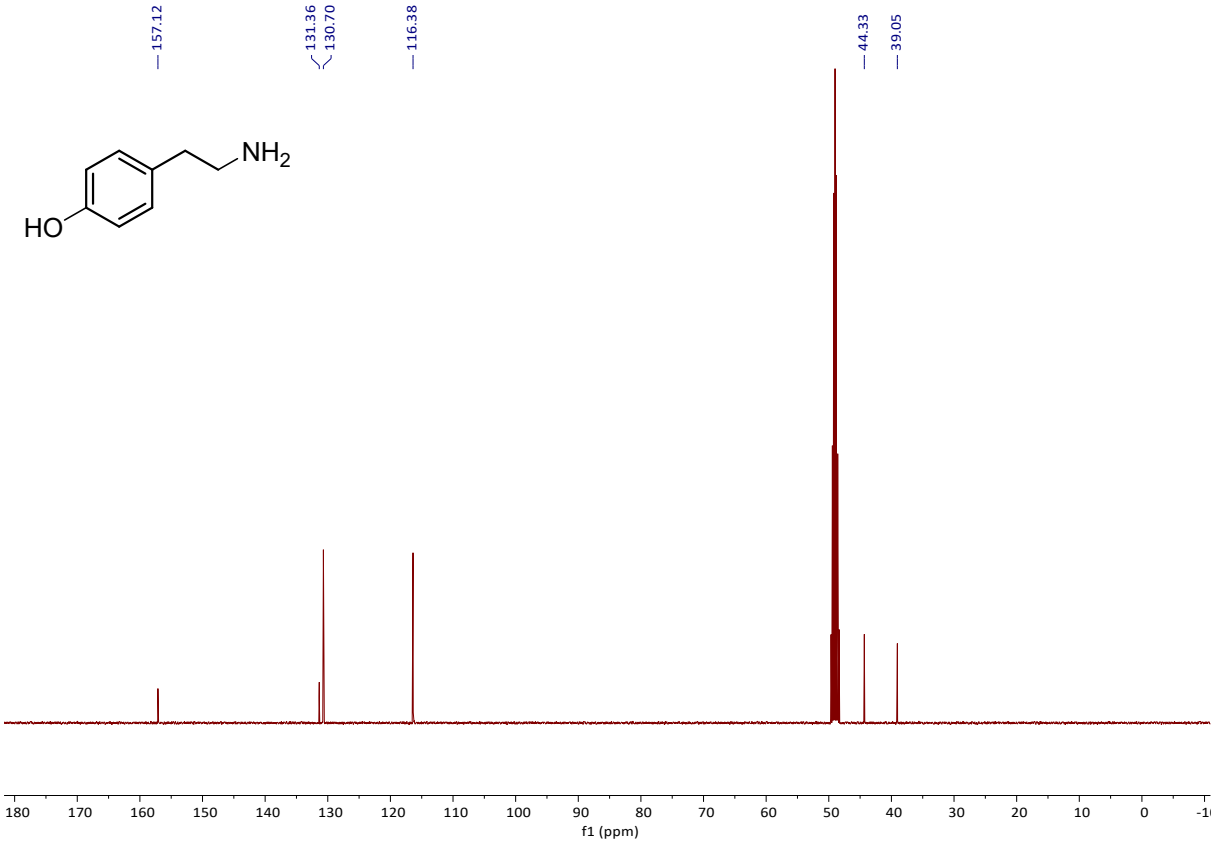

Figure S 28: ^{13}C-NMR (101 MHz, Methanol-d_4) of tyramine (**2i**).

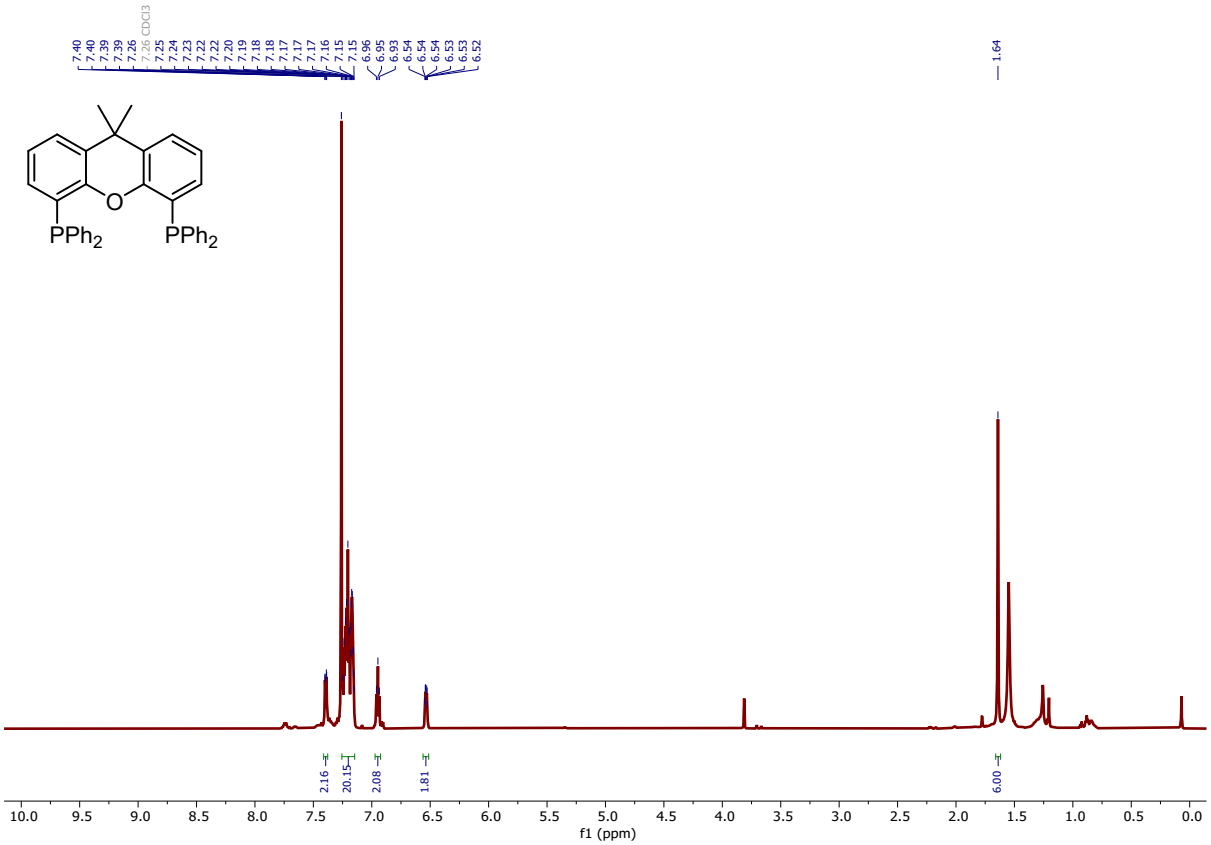

Figure S 29: ^{1}H-NMR (600 MHz, $CDCl_3$) of the precipitated Xantphos ligand.

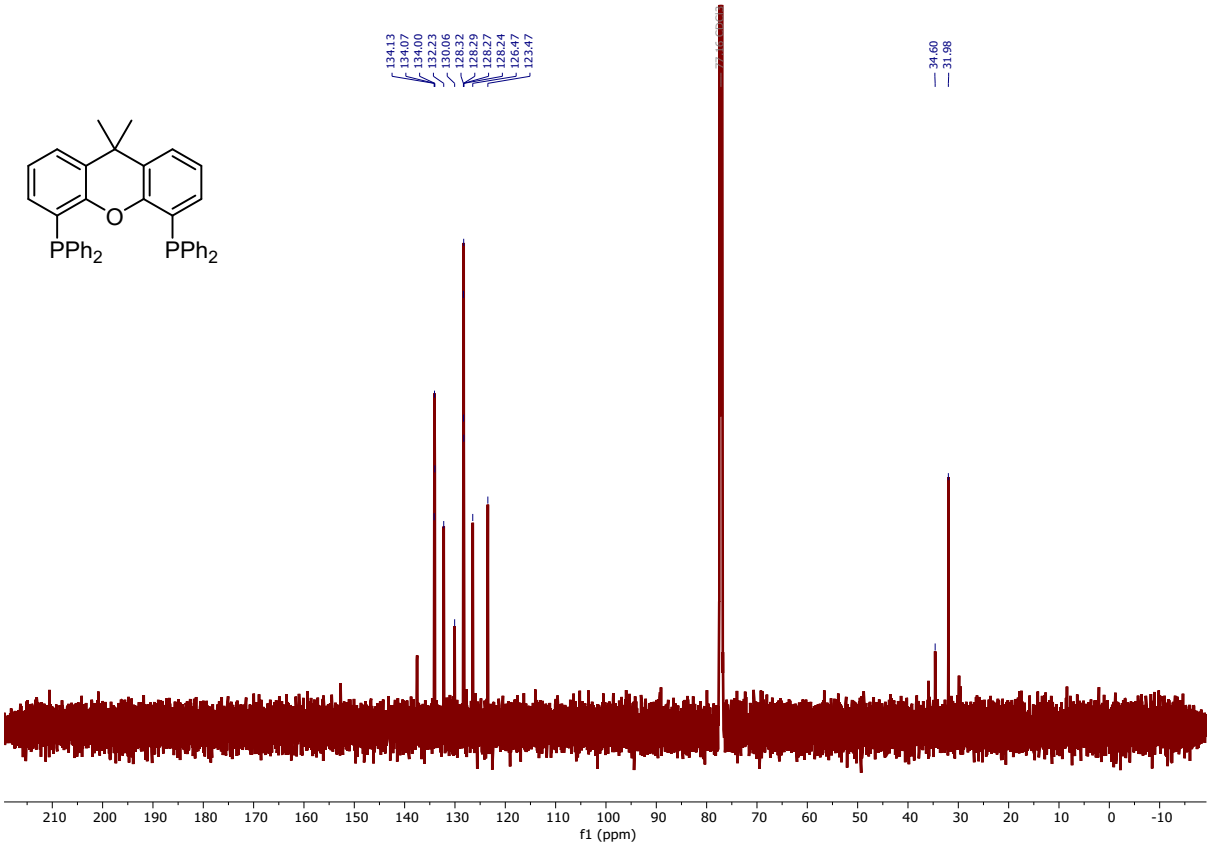

Figure S 30: ^{13}C-NMR (151 MHz, $CDCl_3$) of the precipitated Xantphos ligand.

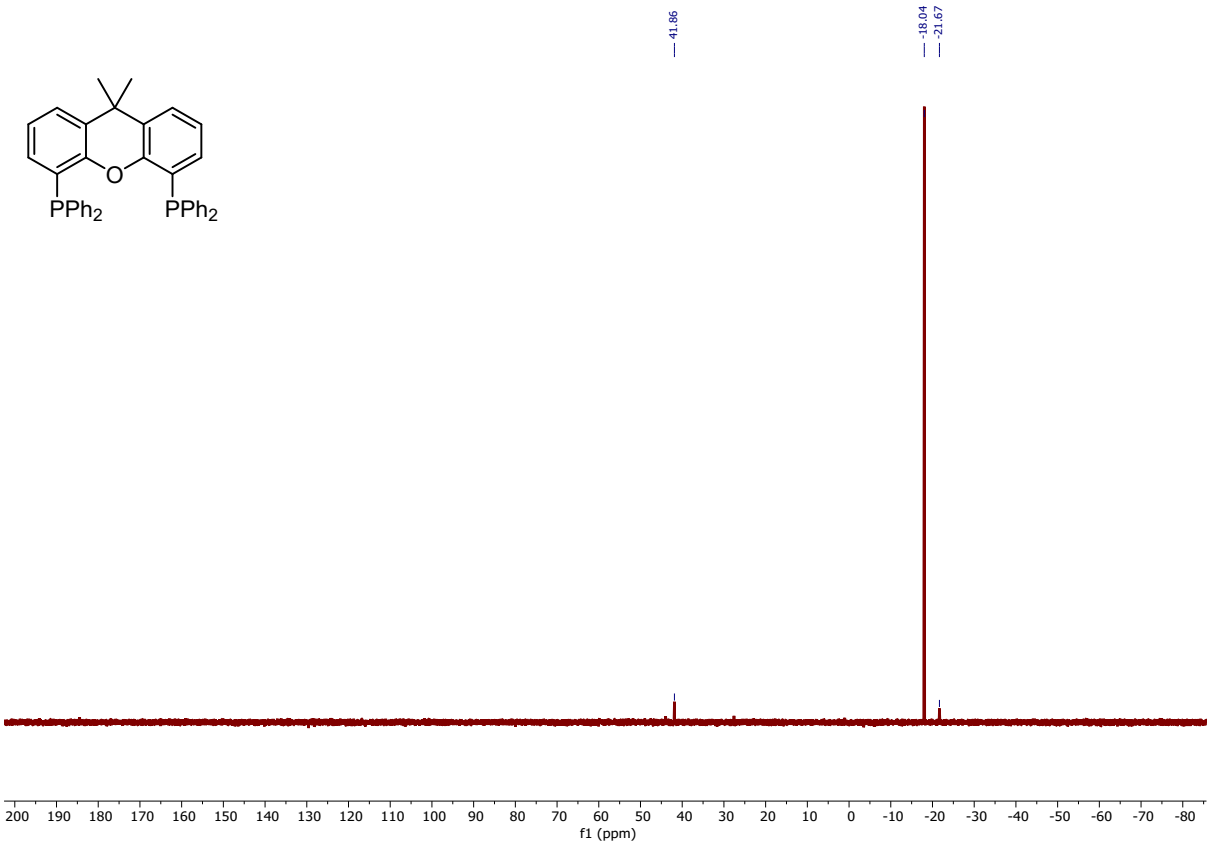

Figure S 31: ^{31}P-NMR (243 MHz, $CDCl_3$) of the precipitated Xantphos ligand.

6. Literature

[1] B. Rienhoff, D. Mede, M. Schöler, D. Vogt, T. Seidensticker, *Chem. Eur. J.* **2025**, *31*, e202500059.

[2] P. V. Ramachandran, A. A. Alawaed, *Molecules* **2023**, *28*, 60.

[3] C. Chen, C. Wang, J. Zhang, Y. Zhao, *J. Org. Chem.* **2015**, *80*, 942.

[4] C. Zhou, D. Singh, B. A. Arndtsen, *Angew. Chem. Int. Ed.* **2025**, *64*, e202423519.

[5] Y. Shi, P. C. J. Kamer, D. J. Cole-Hamilton, *Green Chem.* **2017**, *19*, 5460.

[6] C. Rosso, R. Birolo, A. Gallo, W. T. Franks, E. Priola, M. R. Chierotti, R. Gobetto, *Chem. Eur. J.* **2025**, *31*, e202500080.

[7] H. Unbehauen, *Regelungstechnik I. Klassische Verfahren zur Analyse und Synthese linearer kontinuierlicher Regelsysteme, Fuzzy-Regelsysteme*, Vieweg+Teubner, Wiesbaden, **2008**.

[8] R. Habermann, *Dissertation*, Universität Paderborn, Paderborn, **2005**.

[9] A. E. Rodrigues, *Chem. Eng. Sci.* **2021**, *230*, 116188.